Title

REACTIONS OF MODULATED MOLECULAR BEAMS WITH PYROLYTIC GRAPHITE II. OXIDATION OF THE BASAL PLANE

Authors

Olander, D.R.
Siekhaus, W.
Jones, R.
et al.

Publication Date

1971-10-01

Submitted to Journal
of Chemical Physics

LBL-190
Preprint

REACTIONS OF MODULATED MOLECULAR BEAMS WITH PYROLYTIC GRAPHITE
II. Oxidation of the Basal Plane

D. R. Olander, W. Siekhaus, R. Jones, and J. A. Schwarz

October 1971

AEC Contract No. W-7405-eng-48

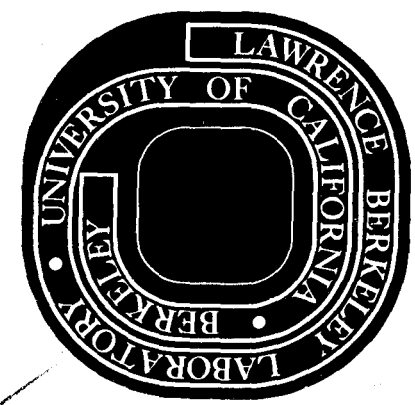

LBL-190

DISCLAIMER

REACTIONS OF MODULATED MOLECULAR BEAMS WITH PYROLYTIC GRAPHITE

II. Oxidation of the Basal Plane

by D.R. Olander, W. Siekhaus, R. Jones, and J.A. Schwarz
Inorganic Materials Research Division
of the Lawrence Berkeley Laboratory and the
Department of Nuclear Engineering
University of California, Berkeley, California 94720

ABSTRACT

Reaction of molecular oxygen as a modulated molecular beam with the basal plane of pyrolytic graphite was investigated.

The graphite surface participated in the reaction in an unusual fashion. Oxidation tends to create a highly reactive surface while thermal annealing tends to deactivate the surface. The imbalance of these two competing processes results in slow changes in surface reactivity during the course of an experiment, which is manifest as hysteresis in the rate of CO production. The surface chemical reaction occurs on a much smaller time scale than the processes responsible for hysteresis. The data indicate that a two-branch, two-site mechanism explains both the hysteresis and the surface chemistry. Surface migration of adsorbed oxygen is shown to be a step in the production of CO. Carbon dioxide was barely detectible; its production rate was two orders of magnitude smaller than that of carbon monoxide at all temperatures.

I. INTRODUCTION

A modulated molecular beam technique has been used to study the low pressure, high temperature oxidation of the basal plane surface of pyrolytic graphite. The primary products of the reaction (CO and CO_2) were monitored mass spectrometrically using the phase lock detection technique described in Part I of this series.[1] Independent control of the reactant gas temperature and pressure, surface temperature, and modulation frequency of the reactant oxygen beam enabled us to probe the surface processes in greater detail than would have been possible by the conventional techniques of heterogeneous kinetics.

As early as 1915, the first attempt to elucidate the mechanism of the oxidation of carbon was made by Langmiur.[2] Since then, many studies of the kinetics of this reaction have appeared in the literature.[3-10] The practical interest in the carbon-oxygen system stems from the refractory nature of carbon, which makes it well suited for devices that are subjected to high temperatures and corrosive environments. Our purpose, however, is to understand the mechanism of the oxygen-graphite reaction.

With growing interest in working with well-characterized specimens, oxidation has been studied using naturally occuring graphite single crystals. Such crystals, although too small for burning to yield gross dimensional changes, are ideal for microscopic examination.[11-14] Thus, studies of the surface morphology changes accompanying oxidation have indicated that sites of preferred attack can often be identified.[15] Observations of the growth of oriented etch pits have been used to estimate the rates

of oxidation in different crystallographic directions and to speculate on the nature of the elementary steps involved in the oxidation process.[16]

II. EXPERIMENTAL

The experimental apparatus, target preparation, detection technique, signal processing, and the method of relating reaction models to the measured apparent reaction probabilities and reaction phase lags was described in Part I of this series.

Ultra high purity oxygen gas was used in the oxidation studies. The manufacturer-supplied analysis of this gas is shown in Table 1. The 4 ppm krypton specification was verified by the mass spectrometer in our reaction system.

III. RESULTS

A. Amplitude Hysteresis

The apparent reaction probability for CO (the most prominent product) for an oxygen beam intensity of 3.4×10^{16} molecules/cm^2-sec modulated at 16 Hz is plotted in Fig. 1. The data exhibit hysteresis behavior similar to that observed by other investigators.[3] Upon continuously increasing target temperature, the apparent reaction probability rises from the noise at $T_s \simeq 1030°K$ and attains a maximum value of nearly 0.01 at $T_s \simeq 1450°K$. From this point to the highest temperature, 1800°K, the reactivity slowly decreases. Upon retracing the temperature path beginning from point C in Fig. 1, the apparent reaction probability follows the lower curve (CDA). The two legs of the loop appear to join

each other at temperatures $<\sim$1150°K, although the loss of reactivity is very drastic in this region and hysteresis would not have been easily observable. We were not able to "close" the hysteresis loop at the high temperature end; the segment CD never retraced the upper portion CB for any measurable temperature span.

While the reaction probability measurements shown in Fig. 1 were obtained, the CO reaction phase lag was also recorded (Fig. 2). The most striking feature of this plot is the complete absence of hysteresis on temperature cycling. We are thus dealing with a case of "amplitude hysteresis" only.

In addition to the presence of hysteresis in the amplitude but not in the phase, these two measured quantities showed another significant difference. The experiments such as those reproduced in Figs. 1 and 2 were repeated a total of four times, upon different days. The phase measurements for each run fell among the points shown on Fig. 2. The reaction probability measurements, however, differed quite a bit from one experiment to another. The best lines through the ε_{CO} data points for the four identical experiments (of which the data of Fig. 1 is one) are shown in Fig. 3. The difference between the various curves is well beyond experimental precision. The shape and location of the amplitude hysteresis loops appeared to depend upon how long it took to do the experiment. None of the CO signal amplitude points was very stable - they appeared to be drifting slowly with time. The phase angles, however, were quite stable.

All four experiments were performed on the same pyrolytic graphite target.

Two experiments were performed to further explore the phenomenon of amplitude hysteresis.

(1) The Annealing Experiment

With the oxygen beam on at all times, a sample was brought from low temperature up to T_s=1450°K (near the peak point B in Fig. 1). All experimental parameters were then held constant and the behavior of the CO signal amplitude with time was observed. It was found that the signal slowly decreased from point B toward point D, where it stopped. The decay of the CO signal is approximately exponential in time and the data plotted on Fig. 4 permitted a mean life of 40 min. to be deduced. In two mean lives, the CO signal decay is 87% complete. In this interval, 5×10^{17} carbon atoms/cm^2, or 125 basal plane layers, were removed. This burn-off corresponds to removal of 9×10^{-7} gm-atoms C/cm^2, which compares favorably with the value of 3×10^{-7} gm-atoms C/cm^2 obtained by Duval[3] for the removal of super-reactivity in his samples.

From this experiment, we conclude that: (a) the process responsible for the observed amplitude hysteresis is sluggish compared to the time scale of the surface reactions, which must occur on the time scale of the beam modulation to be observable by the ac phase-sensitive detection method. The modulation times are typically 100 msec, which is four orders of magnitude smaller than the characteristic time of surface reactivity change. (b) The lower curve in Fig. 1 corresponds to the

"stationary" state; the upper portion of the loop represents a temporary state of super-reactivity.

(2) The Activation Experiment

The second experiment was begun with a sample undergoing reaction on the lower branch of the hysteresis loop (say between points C and D in Fig. 1). The temperature was reduced to T_s=1125°K (approximately where the branches of the hysteresis loop join) and held at this temperature for different amounts of time under two conditions: (a) reactant beam on and (b) reactant beam off. After this "cooking" period, the temperature was returned to T_s≃1450°K (points B or D in Fig. 1) and the CO signal was measured.

The results of the experiment just described are shown in Fig. 5. The times in parentheses indicate the "cooking" time at 1125°K. If the beam was off during cooking, return from the low temperature to 1450°K followed the lower branch of the hysteresis loop; when the oxygen beam was on during the cooking interval, the oxidation rate at 1450°K was in the vicinity of the upper branch of the hysteresis loop. Moreover, the CO signal at 1450°K was higher the longer the sample was cooked in oxygen at the low temperature. From these observations we conclude that the oxidation process itself causes the reactivity of the surface to increase.

The hysteresis in amplitude is believed to be a manifestation of slow variations in the reactivity of the graphite surface, which is driven in opposite directions by two phenomena: (1) The oxidation process, which produces a reactive surface and (2) thermal annealing, which deactivates the surface. At low temp-

eratures (roughly to the right of the peak at B in Fig. 1), thermal annealing is very slow, but the reaction rate is appreciable; the surface tends to become activated by oxidation in this region. At higher temperatures (to the left of point B), thermal annealing begins to compete successfully with oxidative activation of the surface, and it is possible to slowly anneal out the excess reactivity introduced at low temperatures. At very high temperatures (which our experiment could not reach) hysteresis would be expected to disappear because thermal processes alone would control the activity of the surface.

Qualitatively, the amplitude hysteresis loop of Fig. 1 arises from the following sequence of events: as the target temperature is raised from point A, the oxidation process generates reactivity at a rate which the still slow thermal annealing processes are unable to destroy. Consequently, the surface becomes excessively reactive as the temperature is raised from A to B, the extent of the excess reactivity depending upon the time spent going from A to B and the oxygen beam intensity. The reaction probability levels off at B primarily because the production of CO is limited by the rate of arrival of O_2 at the surface (i.e., all of the oxygen which "sticks" on the surface reacts). This phenomenon would normally result in a plateau of constant reaction probability over a substantial temperature range (as in the case of H_2 dissociation on a metal[17]). However, the plateau does not occur in the present case because, in addition to arrival-limited reaction, the surface reactivity decreases due to the onset of appreciable thermal annealing

between points B and C.

In the return path CDA, excess reactivity is not present. As noted above, excess reactivity is produced only at low temperatures, and its effect has been largely destroyed by the high temperature annealing which occurs while the sample is at point C. Thus, the return path from C to D is one of "normal" reactivity, but excess reactivity is generated during the temperature descent from D to A. Thus, excess reactivity may be generated either during cooling from D to A or while heating from A to B. The hysteresis loops for apparently identical experiments are different (see Fig. 3) because the time spent at various points of the cycle was not controlled, and undoubtedly differed from one experiment to another.

We have not yet described what the rather imprecise term "reactivity" means. We postpone this discussion until later, but at this time indicate that we believe it pertains to the nature of the graphite surface proper, probably in its content of point defects or kinks and ledges but perhaps also its roughness. In these experiments, it is clear that the surface participates in the overall reaction in a much more complex fashion than passively supplying the atoms to make product molecules. Fortunately, the response of the surface is much more sluggish than the speed of the chemical reaction, so that separation of the two effects is possible.

B. Effect of Beam Intensity

The variation of the CO signal amplitude with beam intensity (equivalent oxygen pressure at the surface)

was determined at several temperatures in the range 1030-1800°K. The results are shown in Fig. 6, where CO signal and oxygen beam intensity are plotted on logarithmic scales. The signal amplitude has been arbitrarily scaled and the data at each surface temperature have been placed conveniently above each other in proceeding to higher temperatures. If the otherwise useful apparent reaction probability, ε_{CO}, had been plotted, the upper curves would have been awkwardly intertwined because of the maximum in the ε_{CO}-T_s plot of Fig. 1.

The slope of the curves drawn through the data (which will be discussed later) gives the effective order of the reaction with respect to oxygen pressure. At high temperatures ($\gtrsim$1200°K), a first order reaction is observed, but as the temperature is reduced, the reaction begins to obey progressively lower order kinetics. The low temperature kinetics are not of the simple power-law type, however, since the lines of Fig. 6 are distinctly curved. The apparent order of the reaction at the lowest temperature studied is less than one half. Pressure hysteresis, as described by Duval,[3] was not observed.

C. Effect of Beam Temperature

The reaction rate was measured as a function of the temperature of the incident beam. The Arrhenius plot of the CO signal versus beam temperature in Fig. 7 shows essentially zero slope at both surface temperatures investigated. Assuming that a beam molecule makes only one collision with the surface before reacting or scattering, these results suggest that the kinetics of the surface reaction are independent of the thermo-

dynamic state of the reactant gas. The surface processes do not depend upon the translational energy of the incident O_2 molecules or the proportion which are in excited rotational or vibrational states.

D. Frequency Scan

Figs. 8 and 9 show the variation of ϕ_{CO} and ε_{CO} with frequency at T_s=1305°K.

The reaction phase lag (Fig. 8) is seen to vary slowly with the modulation frequency. This observation is of central importance in determining a reaction mechanism, for it demonstrates that the reaction cannot be proceeding by a simple O_2 adsorption - CO desorption mechanism, such as: $O_2(g) \rightarrow 2CO(ads) \rightarrow 2CO(g)$. This reaction is formally described by the simple (i.e., non-reactive) adsorption-desorption analysis presented in Part I (see Sec. IIIC). If, as in Fig. 8, the reaction phase lag is 10° at 50Hz, then Eq(20) of Part I shows that at a frequency of 500 Hz, the phase lag should have been 60°, whereas the observed phase lag at 500 Hz is only 25°.

The observed insensitivity of phase behavior to modulation frequency is indicative of a branched process consisting of a fast and a slow step in parallel. It is a general feature of such processes that the phase lag may be quite insensitive to modulation frequency. Essentially, the signal is a vector sum of the signals from the fast and slow branch. At low frequencies both branches act at full strength at zero phase, but as the frequency is increased the slower process begins to be demodulated - losing amplitude and exhibiting a phase lag. The phase lag of the

total (sum) signal increases also. Eventually, demodulation becomes so severe that the slow process contributes nothing. Of course, the faster process sooner or later becomes demodulated and follows the same course as its slower partner. If the two branches proceed at rates separated by a factor of 10, or so, the combination of the two branches maintains a fairly flat phase response over a wide frequency range. The curve in Fig. 8 marked "theory" is based upon a mechanism which incorporates a two-branched process (Sec. IV).

In addition to insensitivity of reaction phase lag to modulation frequency, the apparent reaction probability of a two branch process should also be a slowly decreasing function of modulation frequency. Fig. 9 shows that this expectation is confirmed.

E. Detection of CO_2 Reaction Product

Only a small amount of CO_2 was produced by the reaction. The CO_2 signal was usually two orders of magnitude smaller than the CO signal. Because the signals were near the limit of detectability, only a few experiments measuring CO_2 production were performed. Fig. 10 shows the variation of the apparent reaction probability as a function of surface temperature. It is clear that the CO_2 yield is not decreasing with increasing temperature, as a purely thermodynamic argument[18] would suggest.

The CO_2 reaction phase lag corresponding to the apparent reaction probabilities shown in Fig. 10 were exceedingly difficult to measure, but appear to be $\sim 30°$, independent of temperature.

Fig. 11 shows a plot of the CO_2 signal vs. oxygen beam intensity at constant frequency and surface temperature. To within experimental accuracy, the production of CO_2 is first order in oxygen beam intensity.

IV. REACTION MECHANISM

The method of interpreting data obtained in a modulated molecular beam experiment follows the sequence:

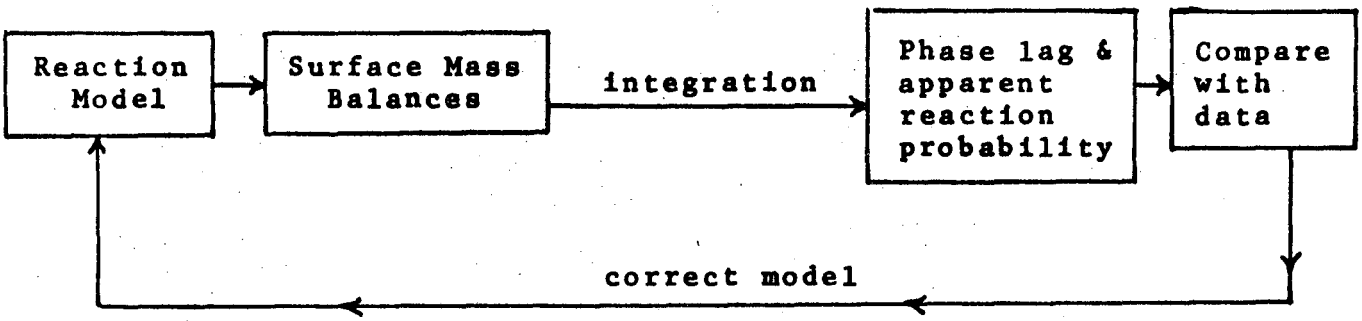

The process of translating a proposed mechanism into a reaction phase lag (ϕ) and an apparent reaction probability (ε) which may be compared with experiment is quite tedious for non-linear processes. Consequently, we have developed the following criteria for selecting likely mechanisms without extensive cut-and-try efforts.

First, the model should reflect the qualitative features of the data. This type of gross agreement of model and data usually can be discerned before detailed model calculations are performed.

Second, the model should have the smallest number of adjustable constants to fit the available experimental data. Each of the constants should describe some elementary process (e.g., desorption, surface migration). The numerical values of the constants obtained

by fitting the data to the model should be physically reasonable.

The aspects of the present data which may be compared with potential mechanisms are:

(1) The reaction phase lag at high temperatures is less sensitive to modulation frequency than expected for a one step kinetic process. Thus, we seek models with two parallel routes for producing the CO reaction product.

(2) Although the reaction is first order at high temperatures, at lower temperatures the kinetic order is less than one and not of the simple power law type. Behavior such as this suggests that the primary act of oxygen chemisorption is reduced by the coverage of active centers on the surface by bound CO. When the surface is completely covered with product (which occurs at low temperatures), the apparent reaction order would be zero. When the temperature is sufficiently high to rapidly desorb all product CO as it is formed, the reaction would be first order in beam intensity.

The general notions expressed by (1) and (2) above are in accord with the model of graphite oxidation proposed by Strickland-Constable.[4] However, the two branches in his model are both of the reactive adsorption-desorption type. Our results, on the other hand, suggests that the two branches are of different character.

(3) The hysteresis phenomenon discussed in Sec. IIIA occurs in signal amplitude but not phase. Hysteresis suggests that there are two types of active sites involved in the reaction.

A. Reaction Model

Oxygen chemisorbs on A-type sites to form a bound CO and at the same time releases the partner oxygen atom as a mobile adsorbed species. The oxygen atom deposited on the surface in this fashion does not desorb to the gas phase (its binding energy is ∿100 kcal/mole,[19] which makes its mean residence time on the surface quite large). Neither does it recombine with another migrating O atom to reconstitute O_2 - if such a process were important, the reaction would have been non-linear (since it would require an elementary step with a rate proportional to the square of the surface concentration of adsorbed atomic oxygen). Yet in the 600° range from 1200-1800°K, the CO signal was proportional to the oxygen beam intensity. Thus, the only remaining route for the adsorbed atomic oxygen is reaction to form CO. We expect that the adsorbed oxygen atom is free to migrate over the surface and find a B-type site with which to react to form bound CO. The CO on the surface, formed either on A sites by direct O_2 chemisorption or subsequent to migration of adsorbed oxygen atoms to B sites, desorbs to provide the signal monitored by the mass spectrometer.

To provide a net generation of A sites (as required for hysteresis), we assume that upon release of CO from a B site, that a fresh A site may be created. Only a small fraction of the

B sites need to be converted to A sites as a consequence of CO desorption in order to provide a net production of A sites at the rates characteristic of the response times of the surface (Sec. IIIA). The conversion of some B sites to A sites by desorption of CO is responsible for the increased reactivity generated by oxidation. This site conversion feature is also shared with the Strickland-Constable model.[4]

These processes are summarized by the reaction mechanism:

$$O_2(g) + S_A \xrightarrow{\eta} \begin{cases} (CO)_{ads} \xrightarrow{k_d} CO(g) + S_A \\ O_{ads} + S_B \xrightarrow{k} (CO)_{ads} \xrightarrow{k_d} CO(g) + S_A \text{ or } S_B \end{cases} \qquad (1)$$

The rate of the first step is governed by the intensity of the molecular beam and the sticking probability η, which is the probability that an O_2 molecule impinging on the surface interacts strongly enough to form the species O_{ads} and $(CO)_{ads}$. The fraction $1-\eta$ of the impinging O_2 molecules which do not interact in this fashion are scattered from the surface. Sticking can occur only upon certain active regions of the surface, which we have called A sites. Moreover, the A site cannot be harboring a bound CO if it is to be able to dissociatively adsorb an incoming O_2 molecule. The reduction of η due to coverage of A sites is responsible for the departure from first order kinetics at low temperature.

A number of theoretical[20,21] and experimental[22,23] studies have been made in an attempt to describe the analytical form of

the coverage dependence of the sticking probability of simple gases on metal surfaces. We do not need to consider the forms which require adjacent unoccupied sites for simultaneous adsorption of both partners of a diatomic molecule. In our model, only one oxygen atom is bound to the site while the other is mobile, hence only one free A site is needed for chemisorption of the O_2 molecule. Formulas such as the one proposed by Kisliuk[20,21] are computationally difficult and involve more than one adjustable constant. Therefore, we have chosen to represent the coverage dependence of the sticking probability by the simple linear function:

$$\eta = \eta_o(1-n_A/N_A) \qquad (2)$$

where η_o is the sticking probability on a bare surface, n_A is the surface concentration of CO bound on A sites and N_A is the total number of A sites per cm^2 of surface (occupied or not). The sticking probability in the limit of zero coverage is written as the product of a cross section and the density of A sites:

$$\eta_o = \sigma N_A \qquad (3)$$

The bare surface sticking probability η_o has been broken

down into the two factors σ and N_A because the long term changes in the latter quantity are believed to be responsible for hysteresis. Consequently, the cross section σ, and not the bare surface sticking probability η_o, is the invariant property of the surface. The cross section may be visualized as an area of the surface surrounding an A site upon which the O_2 chemisorption process can occur. Possible orientation requirements on an impinging O_2 molecule (i.e., a steric factor) are also included in the cross section, so that σ may not represent a real area of the surface.

The CO desorption step is pictured simply as removal of the bound species from the surface to the gas phase as a result of thermal fluctuations which occasionally supply sufficient energy to rupture the bond between CO and the surface. Thus, the pre-exponential factor of the desorption rate constant k_d should be on the order of 10^{12}-10^{13} sec^{-1} and the activation energy of k_d should represent the binding energy of CO on graphite. It is possible that the desorption rate constants for the two branches might be different. We have not permitted this degree of flexibility in the model since it would have introduced two additional constants to be determined from the data.

The first order rate constant k describes the migration of adsorbed oxygen atoms from A sites where they are created to B site where reaction to form bound CO occurs. Justification of this interpretation is presented in Sec. VD. For the present, k may be regarded simply as the first order rate constant which governs the reaction of O_{ads} with B sites to form bound CO.

B. The Surface Mass Balances

The reaction model just described is combined with mass balances on each identifiable intermediate in the reaction. In the present model, there are three surface intermediates: O_{ads}, with surface concentration n'; and CO bound to A and B sites, with surface concentrations denoted by n_A and n_B, respectively. The mass balances on these species are:

$$\frac{dn'}{dt} = \sigma N_A I_o (1-n_A/N_A) g(t) - kn' \qquad (4)$$

$$\frac{dn_A}{dt} = \sigma N_A I_o (1-n_A/N_A) g(t) - k_d n_A \qquad (5)$$

$$\frac{dn_B}{dt} = kn' - k_d n_B \qquad (6)$$

By Eqs(2) and (3), the group $\sigma N_A(1-n_A/N_A)$ is identified with the sticking probability η, and the first term on the right hand sides of Eqs(4) and (5) represent the rate at which the reactant molecules supply O_{ads} and $(CO)_A$ to the surface. The modulated supply of reactants is a consequence of the gating function g(t), which is periodic with a repetition time on the order of tens of milliseconds. We know from the discussion of hysteresis that the site density N_A is a slowly varying function of time. We may uncouple long-term A site annealing or growth from the rapid response of the surface reaction intermediates to the modulated reactant beam because the difference in the time constants of these two processes is very large. Therefore, we assume that the site density N_A does not change significantly over

the period of one modulation cycle, which is the interval over which Eqs(4), (5) and (6) are integrated.

Since the surface mass balances contain non-linear terms, the "brute force" technique of calculating the response of the reaction system to the modulated beam must be used.[24] The beam arriving at the target is nearly square-chopped, so that g(t) may be taken as unity during the "on" portion of the modulation cycle ($-\frac{\pi}{\omega} \leq t \leq 0$) and zero during the "off" portion ($0 \leq t \leq \frac{\pi}{\omega}$).

Eqs(4)-(6) may be solved sequentially. Eq(5) is first solved for the concentration n_A during the off and on periods. This solution is then used in Eq(4) to determine n' and finally Eq(6) is integrated to yield n_B. The results are:

$$\frac{n_{A(on)}}{N_A} = \frac{1}{1+Z} + c_1 e^{-k_d(1+Z)t} \tag{7}$$

$$\frac{n_{A(off)}}{N_A} = d_1 e^{-k_d t} \tag{8}$$

$$\frac{n_{B(on)}}{N_A} = \frac{1}{1+Z} - \left(\frac{\gamma}{1-\gamma+Z}\right) c_1 e^{-k_d(1+Z)t} + \frac{\gamma}{1-\gamma} c_2 e^{-kt} + c_3 e^{-k_d t} \tag{9}$$

$$\frac{n_{B(off)}}{N_A} = \left(\frac{\gamma}{1-\gamma}\right) d_2 e^{-kt} + d_3 e^{-k_d t} \tag{10}$$

where

$$Z = \sigma I_o / k_d \tag{11}$$

$$\gamma = k/k_d \tag{12}$$

The solutions for $n'_{(on)}$ and $n'_{(off)}$ are not shown, but involve the same parameters as the solutions for n_A and n_B. The constants $c_1 \ldots d_3$ are determined by the cyclic matching conditions, which require that:

$$n_{(on)}(0) = n_{(off)}(0) \tag{13a}$$

$$n_{(on)}(-\frac{\pi}{\omega}) = n_{(off)}(\frac{\pi}{\omega}) \tag{13b}$$

where n represents n_A, n_B, or n'. There are six matching conditions which suffice to fix the six constants of integration.

The rate constants k and k_d may be expressed in Arrhenius form by:

$$k = Ae^{-E/RT_s} \tag{14}$$

$$k_d = A_d e^{-E_d/RT_s} \tag{15}$$

where A and A_d are frequency factors, E and E_d are activation energies, R is the gas constant and T_s is the temperature of the surface. The time variation of the surface concentrations n_A and n_B over a modulation cycle are determined in terms of three experimentally controllable variables, ω, T_s and I_o, and the six

parameters of the model:

pre-exponential factors A and A_d

activation energies E and E_d

A-site cross section σ

A-site density N_A.

The rate of CO desorption from the surface is $k_d(n_A+n_B)$, of which only the first Fourier component is required. The fundamental components of the Fourier sine and cosine integrals of the surface concentration are given by:

$$S = \frac{\omega}{\pi}\left\{\int_{-\pi/\omega}^{0}[n_{A(on)} + n_{B(on)}]\sin\omega t dt + \int_{0}^{\pi/\omega}[n_{A(off)} + n_{B(off)}]\sin\omega t dt\right\} \tag{16}$$

$$C = \frac{\omega}{\pi}\left\{\int_{-\pi/\omega}^{0}[n_{A(on)} + n_{B(on)}]\cos\omega t dt + \int_{0}^{\pi/\omega}[n_{A(off)} + n_{B(off)}]\cos\omega t dt\right\}$$

Finally, the apparent reaction probability and reaction phase lag are given in terms of the Fourier sine and cosine integrals by:

$$\varepsilon_{CO} = \frac{k_d}{I_o\bar{g}}(S^2 + C^2)^{1/2} \tag{17}$$

$$\phi_{CO} = -\tan^{-1}(C/S) \tag{18}$$

$\bar{g}$ is the first Fourier component of the gating function ($2/\pi$ for

a square chopped beam). Additional details of the solution method are given in Ref. 25.

C. Determination of the Kinetic Parameters

Although the reaction model contains six parameters, the wide range of experimental variables afforded by the modulated molecular beam technique permits selection of experimental conditions in which only one or two of the parameters govern the overall reaction. In addition, simpler solutions for ε_{CO} and ϕ_{CO} are obtainable in the temperature region where the overall process is first order.

(1) The Surface Migration Rate Constant

At high temperatures, the surface concentration of bound CO is low because the desorption rate constant k_d is large. Consequently, the non-linear term n_A/N_A in the surface mass balances of Eqs(4) and (5) may be neglected compared to unity. The linear equations may be readily solved by the techniques developed in Part I, from which the apparent reaction probability and reaction phase lag are found to be:

$$\varepsilon_{CO} = \sigma N_A \frac{b}{\sqrt{1+a^2}} \tag{19}$$

$$\phi_{CO} = \tan^{-1} a \tag{20}$$

where

$$a = \frac{\left[1 + 2\left(\frac{k}{k_d}\right) + \left(\frac{k}{k_d}\right)\left(\frac{\omega}{k_d}\right)^2\right]\left(\frac{\omega}{k}\right)}{2 + \left(1 - \frac{k}{k_d}\right)\left(\frac{\omega}{k}\right)^2} \tag{21}$$

$$b = \frac{4 + \left(\frac{\omega}{k}\right)^2}{2 + \left(1 - \frac{k}{k_d}\right)\left(\frac{\omega}{k}\right)^2} \qquad (22)$$

At low modulation frequencies and over most of the high temperature region, the approximation $k/k_d \ll 1$ may be applied to Eq(21) and the CO phase lag reduces to:

$$\tan \phi_{CO} = \frac{\omega/k}{2 + (\omega/k)^2} \qquad (23)$$

The variation of reaction phase lag with surface temperature at 16 Hz (of which the data in Fig. 2 represent a portion) were used to determine the rate constant k at surface temperatures $\geq$1300°K by application of Eq(23). The results are plotted in Arrhenius fashion in Fig. 12. The best line through the data yields an activation energy of 30±5 kcal/mole and a pre-exponential factor of $2.5 \times 10^7 \text{sec}^{-1}$.

(2) The Desorption Rate Constant at One Temperature

The variation of the reaction phase lag with frequency at 1305°K has been utilized to determine k_d at this particular temperature. Because high modulation frequencies are involved, the ϕ_{CO} was taken from the complete phase expression, Eq(20) and (21), instead of Eq(23). A family of curves of ϕ_{CO} vs ω/k parametric in the ratio k/k_d was constructed and compared to the data shown in Fig. 8. From this graphical comparison, the ratio $(k/k_d)_{1305°K} = 0.02 \pm 0.01$ was found to best fit the data. The curve for this value of the rate constant ratio is marked "theory" on Fig. 8. Determination of k_d at a single temperature by the freq-

uency scan provides a relation between the parameters A_d and E_d of Eq(15).

Use of the known values of k and k_d at 1305°K in Eq(19) provides a check on the variation of the apparent reaction probability during the frequency scan. The curve marked "theory" in Fig. 9 shows such a comparison. The theoretical curve has been scaled to match the data at 16 Hz (since other techniques will be used to determine the bare surface sticking probability in Eq(19)). The rather good agreement on Fig. 9 indicates that the high temperature features of the reaction have been adequately described by the proposed model.

(3) The Desorption Activation Energy and the Chemisorption Cross Section

Determination of the remaining parameters of the model requires examination of the phase lag and reaction probability data in the low temperature region where the process is non-linear. In this region, the coverage n_A/N_A is comparable to unity because the desorption rate constant decreases rapidly with temperature, thus "clogging" the surface with bound CO. The complete mathematical solution described in Sec. IVB, which involves the cross section σ in addition to the parameters k and k_d, is required.

The following method, accomplished by computer, was used to establish the activation energy of the desorption step. A value of E_d was selected and the corresponding value of A_d determined from the known value of k_d at 1305°K. With both rate constants now specified, the apparent reaction probability and reaction phase lag were calculated from the complete solution as a function of

surface temperature for different values of the cross section σ. The combination of E_d and σ which best fit the apparent reaction probability data shown in Fig. 1 and the lowest set of reaction order data of Fig. 6 (at T_s=1030°K) was sought. Heavy reliance was thereby placed upon the lowest temperature measurements because of their sensitivity to the parameters E_d and σ which govern coverage of active sites by bound CO.

Fitting the ε_{CO}-T_s data requires that either the upper or lower branches of the hysteresis loop be chosen a priori as the plateau attained by the theoretical curve. The theory does not include the possibility of variation of the sticking probability with temperature caused by changes in the A site density. However, this phenomenon undoubtedly occurs during the period that both the upper and lower branches of Fig. 1 were measured. We have chosen to match the theory to the lower branch because it represents a stationary state with an A site density which is probably more nearly equal to that in the temperature region where ε_{CO} rapidly falls off from the plateau value.

The fitting procedure yielded values of E_d=50 kcal/mole and σ=75Å^2. The chemisorption cross section corresponds to an active site diameter of 10Å, which encompasses an area equivalent to 15 basal plane hexagons. We estimate that combination of the possible A site density variation in the ε_{CO}-T_s data with uncertainties in surface temperature measurements and beam intensity computations results in an uncertainty of ±5 kcal/mole in E_d and a factor to two in σ.

(4) Concentration of A Sites

The reaction model predicts that the apparent reaction probability should become constant at high temperature. This limit is the dc reaction probability. It may be obtained by setting $\omega/k=0$ in Eqs(19), (21), and (22):

$$(\varepsilon_{CO})_{dc} = 2\sigma N_A \qquad (24)$$

The experimental results of Fig. 1 do not exhibit the predicted plateau because of the slow decrease in N_A due to annealing at high temperatures. Furthermore, N_A is different in each of the four experiments shown in Fig. 3 and for the two branches of each hysteresis loop. A typical value of the A site density is represented by the plateau of the lower branch of the loops shown in Fig. 1, from which we obtain $(\varepsilon_{CO})_{dc} \simeq 5\times10^{-3}$. Using this value and $\sigma=75\text{Å}^2$ in Eq(24) yields an A site density of $3\times10^{11}\text{cm}^{-2}$. On a square pitch, the spacing between A sites is $\sim$180Å.

(5) Summary

The following parameters have been determined by comparing the reaction model proposed in Sec. IVA to the data from the modulated molecular beam experiments:

$$k = 2.5\times10^{7}\exp(-30{,}000/RT_s)\,\text{sec}^{-1}$$

$$k_d = 3\times10^{12}\exp(-50{,}000/RT_s)\,\text{sec}^{-1}$$

$$\sigma = 75\text{Å}^2$$

$$N_A \simeq 3\times10^{11}\ \text{sites/cm}^2$$

V. DISCUSSION

A. Agreement Between Theory and Experiment

When used in the mathematical model of the reaction, the values of the parameters of the reaction model summarized above produce the theoretical curves in Figs. 2, 6, 8, and 9. The curves drawn in Fig. 1 are not based upon theory. Fig. 13 compares the computed values of ε_{CO} with the data on the lower branch of Fig. 1. The decrease of ε_{CO} at high surface temperatures is not included in the model, which assumes a single value of N_A.

The generally good agreement between the theory and the data warrants acceptance of the broad outlines of the proposed model. In addition to the troublesome long-term variations in the A site density (which affects all ε_{CO} measurements), the model has other weak points. It does not even closely reproduce the very distinct phase lag maximum evident in the data of Fig. 2 - the best the theory can do is a sort of wiggle at the temperature where the maximum occurs. However, the decrease in ϕ_{CO} occurs in the very low temperature region from 1100 to 1030°K where, according to Fig. 1, the signal amplitudes are an order of magnitude less than the maximum values. The phase measurements of these weak signals are the least reliable. Also, theoretically predicted phase lags are very susceptible to minor ommissions in the model. It is quite possible that the decrease in the phase lag below 1100°K is due to another mechanism for CO production (not included in the model) which occurs rapidly (zero phase lag) but in small quantities. As the larger (but slower) component becomes demodulated, the smaller, fast component could reduce the total phase angle of the signal, thereby causing the maximum in Fig. 2.

It is possible that a more realistic description of the coverage dependence of the sticking probability than the simple linear function of Eq(2) may have given better agreement with the low temperature phase lag measurements.

It has been our experience with model calculations that the reaction phase lag is the quantity which is the most sensitive to either small alterations in the model or to small changes in the parameters of a model. This extreme sensitivity of the phase lag is an advantage in that it readily permits elimination of many potential mechanisms, but it is a disadvantage in that it is very difficult to obtain quantitative agreement with phase lag data unless the model is practically perfect. Nonetheless, the phase lag is more valuable than the reaction probability for analyzing the data from a modulated molecular beam experiment for the reason mentioned above and also because it does not depend upon the bare surface sticking probability, as does ε_{CO}.

B. Generation and Annealing of A-Sites

We examine the response of the A site density to the oxidation process and to temperature changes. Our object is two-fold: First, we wish to demonstrate that the A site density does not respond on the time scale of the modulation, so that the assumption of constant N_A in Eqs(4) and (5) is justified, and second, we wish to describe the long term transients discussed in Sec. IIIA in terms of slow changes in the surface concentration of A sites.

We do not know the specific surface configurations with which the A site may be identified. We know that the A sites are numerous

(the site density of $\sim 3 \times 10^{11}$ inferred from the data corresponds to one A site for every 14,000 surface carbon atoms) and their ability to initiate chemisorption of impinging oxygen molecules is quite long range (having a cross section of 75Å). They are susceptible to creation by oxidation and destruction by thermal annealing processes, which suggests that they are not associated with the emergence of dislocations at the surface.

A surface balance on the total A site density (whether occupied by a bound CO or not) would include the following terms:

(1) Production by thermal processes, at a rate denoted by k^+;

(2) Net generation by the oxidation process.

This source comes from the small fraction δ of the B sites which, as a result of desorption of bound CO, is either transformed to A sites or create A sites. The rate at which B sites react with O_{ads} is kn', and all of the bound CO thus formed ultimately desorbs. Nearly all of such desorption events merely re-open the original B site, but a few generate an A site either in addition to or instead of the original B site. The net rate of oxidative generation of A sites from B sites is $\delta kn'$.

(3) Type A sites may anneal out by a first order process (presumably by diffusion to sinks) described by a rate constant k^- and proportional to the concentration of free A sites.

(4) The A sites may also be removed by annihilation with each other, in a manner similar to the reaction of vacancies and interstitials in the bulk solid. We take this process to be second order in free A sites and described by a rate constant κ.

With these contributions, the surface balance on A sites is:

$$\frac{dN_A}{dt} = k^+ + \delta k n' - k^-(N_A - n_A) - \kappa(N_A - n_A)^2 \qquad (25)$$

The demonstration that the variation in N_A during a modulation cycle is negligible compared to the average A site density on the surface is as follows: If Eq(25) (neglecting the first and last terms on the right hand side for simplicity) is applied to the annealing experiment described in Sec. IIIA, we find that k^- must be on the order of $(40\ \text{min})^{-1}$ or $4\times10^{-4}\ \text{sec}^{-1}$. Since the reactivity of the sample (and hence N_A) decreased in this experiment, the first order annealing term in Eq(25) must have been larger in magnitude than the oxidative generation term. Because of symmetric chopping, the average beam intensity was $\frac{1}{2}\bar{I}_o$. The average value of kn' during this anneal was one half of the oxidation rate, or for an average beam intensity of $\frac{1}{2}(3\times10^{16})$ molecules/cm^2-sec and a reaction probability of $\sim5\times10^{-3}$, we find that $k\langle n'\rangle \sim 4\times10^{13}\ \text{sec}^{-1}\text{cm}^{-2}$. The very fact that the surface reactivity decreased with time despite an oxidation rate of this magnitude means that the fraction δ in the second term on the right of Eq(25) was no greater than:

$$\delta \leq \frac{k^- N_A}{k\langle n'\rangle} = \frac{(4\times10^{-4})(3\times10^{11})}{(4\times10^{13})} \simeq 3\times10^{-6}$$

Thus, only a very small fraction of the bound CO species desorbing from a B site result in creation of an A site.

We can now show that the change in A site concentration over a modulation cycle is small compared to the average density of such sites. When subject to an oxygen beam of intensity 3×10^{16} molecules/cm^2-sec and a probability of producing CO of 5×10^{-3} per O_2 molecule, the number of B sites/cm^2 which release CO during the 5 msec "on" time of a 100 Hz modulated beam is $\frac{1}{2}(3\times10^{16})(5\times10^{-3}) = 4\times10^{11}$. Of this number of B sites which have "processed" a CO species, a fraction 3×10^{-6} transform into an A site, or $\sim10^6$ new A sites/cm^2 are created by the oxidation process during a single modulation cycle. Since the average density of A sites is $\sim3\times10^{11}$, the perturbation on N_A during a modulation cycle is a few parts in a million. The decoupling of Eq(25) from Eqs(4) and (5) is thereby justified. However, were δ on the order of unity, very sizeable shifts in the A site density would have occurred during modulation, and Eqs(4), (5), and (25) would have to have been solved simultaneously by the methods indicated in Sec. IVB.

We turn to the description of the long term variations in A site density. Because of the very large difference in the response times of the surface chemcial processes and the site density, the oxidation rate kn' of Eq(25) may be replaced with its average value over a modulation cycle. The appropriate average may be obtained from Eqs(4) and (5) by setting $g(t) = \frac{1}{2}$ and $dn'/dt = dn_A/dt = 0$ and solving the resulting algebraic equations for the average surface concentrations $\langle n' \rangle$ and $\langle n_A \rangle$. When these results are substituted into Eq(25), there results:

$$\frac{dN_A}{dt} = k^+ + k^- \left[\frac{\frac{1}{2}\delta\left(\frac{\sigma I_o}{k^-}\right) - 1}{1 + \frac{1}{2}\left(\frac{\sigma I_o}{k_d}\right)}\right] N_A - \frac{\kappa}{\left[1 + \frac{1}{2}\left(\frac{\sigma I_o}{k_d}\right)\right]^2} N_A^2 \quad (26)$$

This differential equation describes the change in the concentration of A sites on the graphite surface due to temperature changes or oxidation. A single experiment which produced all of the data shown on Fig. 1 requires on the order of 8 hr, during which time the surface temperature is constantly changed in order to obtain the various data points. At each change in T_s, the rate constants k^+, k^-, k_d and κ acquire different values, and N_A is driven towards a new stationary value in accord with the rate equation of Eq(26). In the experimental program utilized in the present investigation, equilibrium surfaces were not always attained, as evidenced by the existence of hysteresis and by the lack of reproducibility of the hysteresis loops shown in Fig. 3. If sufficient time were allowed at each experimental condition, the surface would have achieved a stationary reactivity and no hysteresis would have been observed. This was impractical, however, since at low temperatures, attainment of an equilibrium surface probably requires many days.

In the following discussion, the last term in Eq(24) will be neglected and it will be assumed that the predominant annealing mechanism is the linear one.*

Whether the A site density tends to increase or decrease is governed by the sign of the quantity in the brackets of the second term on the right of Eq(26). Since k^- is a function of temperature, the bracketed term is zero at a temperature given by:

---

*The quadratic annealing process is required to provide a mechanism for limiting the A site density when the bracketed quantity in the second term on the right of Eq(26) is positive.

$$k^{-}(T^{*}) = \frac{1}{2}\delta\sigma I_{o} \qquad (27)$$

At $T<T^{*}$, the bracketed term in Eq(26) is positive and there is a net growth of A sites by oxidation, which will continue until limited by the quadratic annealing term. For $T>T^{*}$, the linear thermal annealing process is more rapid than oxidative generation of A sites and the bracketed term in Eq(26) is negative. From the experiment described in Sec. IIIA, it was found that sites could be annealed out at T_s=1450°K, but growth of sites occurred with the same beam intensity at 1125°K. Therefore, at a beam intensity of 3×10^{16} molecules/cm^2-sec, T^{*} is somewhere between these two temperatures.

The relation between Eq(26) and the hysteresis phenomenon can be best understood by regarding the procedure followed in obtaining the data as an extremely slow flash filament experiment. The sample is heated from point A in Fig. 1 to point C in a monatonic fashion, although the time constant of the "flash" is on the order of hours rather than milliseconds.

At low temperatures (say $T_s\simeq$1000°K), the rate constants k^{+}, k^{-}, and k_d are all very small and Eq(26) reduces to $dN_A/dt=0$. Or, the A site density characteristic of the previous high temperature history of the sample has been quenched in. As the temperature is raised to the vicinity of point A in Fig. 1, k_d becomes large enough so that measurable quantities of CO are produced (i.e., the group $\sigma I_o/k_d$ is of order ten). The thermal annealing rate constants are still small, but since $T<T^{*}$, the bracketed term in Eq(26) is positive. At some temperature between 1000°K and T^{*}, the

bracketed term in Eq(26) attains its maximum positive value. This is the temperature range in which A sites are created quite readily by oxidation. Passing through this temperature region sufficiently slowly permits the excess A sites required for the upper branch of the hysteresis loop to be generated.

As the surface temperature approaches the value at point B in Fig. 1 the bracketed coefficients of Eq(26) becomes zero and then turns negative. The excess A sites generated by oxidation at low temperature begin to be annealed out. This process continues from B to C. At very high temperatures (not attained in Fig. 1), the bracketed quantity in Eq(26) reduces to -1, and the A site density is completely independent of the oxidation process.

Return of the sample to low temperatures follows the path CDA because the bracketed coefficient of Eq(26) remains negative until the surface temperature drops below T^*, which is probably where the two branches of the hysteresis loop join.

The foregoing explanation of the hysteresis phenomenon closely parallels the description originally presented by Duval[3]. However, the identification of A sites with atomic-size configurations which possess many of the features of point surface defects raises the following conceptual problem. It has been shown that the annealing of A sites requires about 80 min at 1450°K (Sec. IIIA). During this time, the oxygen beam was eroding the target. The burnoff during the transient amounted to 5×10^{17} atoms of carbon/cm^2, or 125 layers of a perfect basal surface. If the A sites are surface entities, how does the supersaturation of the <u>original</u> surface with A sites persist throughout a burnoff of this

magnitude? After a few minutes, the original surface is completely gone, yet the memory that it was supersaturated with A sites is felt in the newly uncovered layers. The answer is that the removal of the bound CO attached to an A site by the act of chemisorption produces another A site in a nearby position in the same layer or in the layer beneath the one which contained the original A site. Thus, the A sites propagate into the solid during burnoff; annealing is simply the occasional disappearance of an A site in the interval between the release of a bound CO and the capture of an impinging oxygen molecule.

C. Surface Roughening

The surface of the single pyrolytic graphite sample used in this study originally had been polished to a high luster. After removal from the vacuum system following several months of experimentation, texturing due to oxidation was evident. The region of the surface which had been heated but which was not illuminated by the primary molecular beam was still shiny. Scanning electron micrographs of the target before and after the experimental program are shown in Fig. 14. Extensive oxidation at the comparatively high temperatures and high rates characteristic of the present study apparently represent conditions far too chaotic to permit formation of the nearly perfect hexagonal etch pits observed in the low temperature oxidation of single crystal flakes of natural graphite.[15] The surface in Fig. 14 strongly resembles the recently discovered "white carbon" allotrope of carbon.[26]

Fig. 14 indicates that the actual area of the surface is undoubtedly considerably greater than the superficial area. Moreover, it is difficult to sustain an argument that the reaction occurs upon perfect basal planes of the graphite lattice, despite the fact that a specimen of this orientation was utilized. The actual surface upon which reaction occurs is so pock-marked that a realistic description of the sticking probability of the bare surface (i.e., free from bound CO) must include the additional area created by roughening, the possibility that a portion of this area is shadowed from direct line-of-sight of the incoming molecular beam, and the possibility of more than one collision with the surface. Thus, instead of Eq(3), the bare sticking probability is probably better described by:

$$\eta_o = RSm[f(\sigma N_A)_{prism} + (1-f)(\sigma N_A)_{basal}] \qquad (28)$$

where:

$$R = \frac{cm^2 \text{ of actual surface area}}{cm^2 \text{ of superficial area}} = \text{roughness factor}$$

$$S = \frac{\text{area illuminated by the molecular beam}}{\text{total area}}$$

m = average number of collisions which a reactant molecule makes with the surface before scattering

f = fraction of the actual surface consisting of prism planes

σ and N_A represent the cross section and A site densities on either the prismatic and basal portions of the surface. "A sites"

denote those active regions capable of dissociatively adsorbing an O_2 molecule. The site densities and cross sections on the two types of surface may be very different. In fact, in view of the widely held view that the prismatic plane is more reactive than the basal plane, $(\sigma N_A)_{basal}$ may be nearly zero and the observed reaction may be occurring only on the portion of the roughened surface containing exposed prism planes.

The quantities S, m, and f are, to a first approximation, functions of the roughness parameter R only. Clearly, when R=1, S=1, m=1 and f=0. As a result of oxidation, the surface may attain a maximum roughness, which corresponds to a minimum value of S and maximum values of m and f. The quantity S is also known as the shadowing function, and has been investigated for certain types of surface roughness by Beckmann (27).

Although the analysis of the hysteresis phenomenon presented in the previous section was based upon variation of N_A only, the effect is in general due to variation in the sticking probability η_o. According to Eq(28), the bare sticking probability can vary either due to changes in N_A or in the roughness factor R, or to both. The limiting case in which R is constant and only N_A varies may be described as the "site annealing" model. The opposite extreme, in which N_A is constant and R varies describes a "surface annealing" model.

In the surface annealing mechanism, oxidation increases reactivity simply by roughening the surface and providing more surface area and hence more A sites in the region of the target illuminated by the molecular beam. The most stable crystallographic

face of pyrolytic graphite is undoubtedly the basal plane, so that the thermal annealing process would tend to smooth out the rough surface and reduce the parameter R. The surface annealing model contains the ingredients needed to provide an explanation of the observed amplitude hysteresis equally as convincing as the site annealing model discussed in the preceding section; in the former model, the top branch of the hysteresis loop is associated with a rough surface and the lower branch with a smooth surface. This mechanism presupposes that a roughened surface of pyrolytic graphite is capable of thermal smoothing on the time scale of hours at temperatures as low as 1500°K. Such an annealing process involves changing the morphology of the entire surface and requires the motion of many carbon atoms. This process seems less likely than the motion of relatively few atomic size defects (the A sites) required in the site annealing model. Moreover, Duval[3] found that although the surfaces of the isotropic graphite he used in his study were indeed roughened by oxidation, the roughness parameter R was not a function of the extent of burnoff; rather, it reached a steady value.

D. Interpretation of the Rate Constant k

The identification of the surface migration step is an example of the usefulness of the phase lag information provided by modulated molecular beam experiments. This step could not possibly have been observed in dc experiments of any kind, since it leads to the same product as the direct, upper branch of the reaction mechanism shown by Eq(1); it simply does so at a different rate.

The frequency scan data of Fig. 8 indicated that both a fast and a slow process were contributing to the CO emission, but did not provide any information about the nature of the two processes. The parameters of the rate constant governing the slower of the two steps were deduced from the phase lag vs. temperature data shown in Figs. 2 and 12 by treatment according to Eq(23). The quantity k in this formula is the rate constant of the slower step, whether it be a desorption, surface migration, or a true "chemical" process. The fact that the pre-exponential factor of k was found to be $\sim 10^{7} sec^{-1}$ quite clearly rules out a simple desorption process, which should have exhibited a pre-exponential factor five or six orders of magnitude larger.

(1) Surface Migration

If the lower branch of the reaction of Eq(1) is a surface migration process, the rate constant k depends upon the surface diffusion coefficient of adsorbed oxygen atoms, D_s, and the density of B sites on the surface, N_B, as can be shown by the following argument: the reciprocal of k is the mean lifetime of an oxygen adatom on the surface. The mean distance over which an oxygen adatom has to migrate to get to a B site is on the order of the spacing of B sites, which is $N_B^{-1/2}$. These two quantities are related to the surface diffusion coefficient by the Einstein formula, which is:

$$(\text{mean distance})^2 = 4D_s(\text{mean time})$$

or $N_B^{-1} = 4D_s/k$. Thus, the rate constant is:

$$k = 4D_s N_B \tag{29}$$

In addition to the brief argument given above, there are several other ways of arriving at formulas differing from Eq(29) only by a multiplicative constant of order unity.[25]

The surface diffusion coefficient is given by:

$$D_s = 6[\tfrac{1}{4}\nu a^2 e^{-E/RT_s}] \tag{30}$$

where ν is the frequency of O atom vibration parallel to the surface and $\underline{a}$ is the length of a diffusive jump. The factor of six outside of the brackets assumes that there are six equivalent jump directions from a surface location containing an O_{ads}.

If the B site density is assumed independent of temperature, the migration energy in Eq(30) may be identified with the activation energy of the rate constant k. Substitution of Eq(30) into Eq(29) and comparison with Eq(14) shows that the pre-exponential factor of k is:

$$A = 6\nu a^2 N_B \tag{31}$$

If a jump frequency of $10^{13}sec^{-1}$ and a jump distance of 2.5Å (the distance between centers of basal plane hexagons) are assumed, the B site density corresponding to $A=2.5x10^{7}sec^{-1}$ is $7x10^{8}sites/cm^2$.

The B site density is ~400 times smaller than the A site density determined previously. This rather substantial difference raises the question of why the migrating O_{ads} cannot react with

the far more numerous A sites in addition to the B sites. (The reaction model used to interpret the data does not contain this variant.) Our only justification for so rigidly segregating the functions of the two types of sites is to explain hysteresis. If A sites could react with O_{ads} to form $(CO)_{ads}$, then the rate constant k would depend upon N_A as well as N_B. However, the appearance of N_A in the rate constant k requires that hysteresis occur in the phase lag as well as in the amplitude of the CO signal. Since only amplitude hysteresis was observed, we are forced to conclude that the agent responsible for hysteresis, namely the A sites, does not affect any of the rate constants which determine the phase lag.

(2) Chemical Reaction

In identifying the first step in the lower branch of the mechanism of Eq(1) with a surface migration process, it was assumed that an adatom merely has to get to a B site in order to form CO. However, if a single collision of an oxygen adatom and a B site is not sufficient to form bound CO, the rate constant k may reflect the kinetics of a slow irreversible reaction between O_{ads} and B sites to produce $(CO)_{ads}$.

The rate of such a reaction may be formulated from absolute rate theory. The transition state is considered to possess an energy E above that of the adsorbed O atom. The partition function of the activated complex (after removing the single degree of translational freedom required by absolute rate theory) is denoted by z^*, which refers to the vibrational and rotational motion of the complex which precedes formation of $(CO)_{ads}$. The number of

sites per unit surface area upon which the activated complex may reside is taken to be equal to the B site density, N_B.

The adsorbed oxygen atoms are assumed to be localized particles with three degrees of vibrational freedom. Inasmuch as the adatom is strongly bound to the surface, the partition function for vibration perpendicular to the surface is set equal to unity. The two degrees of vibration parallel to the surface are characterized by a vibrational frequency ν, so that the partition function for the reactant state is $(1 - e^{-h\nu/kT_S})^{-2}$. The adatom equilibrium positions are assumed to be separated by a distance $\underline{a}$, or there are $1/a^2$ adsorption sites per unit area.

Applying the methods of absolute rate theory to this reaction, the rate per unit area is found to be:

$$\text{Rate} = kn' = \left(\frac{kT_s}{h}\right) \frac{z^*}{\left(1 - e^{-h\nu/kT_s}\right)^{-2}} a^2 N_B n' e^{-E/RT_S} \qquad (32)$$

Or, the pre-exponential factor of the rate constant k is:

$$A = \left(\frac{kT_s}{h}\right) \frac{z^*}{\left(1 - e^{-h\nu/kT_s}\right)^{-2}} a^2 N_B \qquad (33)$$

Since the universal frequency factor kT_s/h is approximately 10^{13}sec^{-1}, and since the partition function ratio $z^*/(1 - e^{-h\nu/kT_s})^{-2}$ is probably of order unity, Eq(33) is very nearly equivalent to Eq(31). Therefore, we cannot decide on the basis of the magnitude of the pre-exponential factor alone whether the first step in the lower branch of the mechanism of Eq(1) represents surface migration

of O_{ads} to B sites or the reaction between these entities to form bound CO. However, the substantial activation energy of 30 kcal/mole seems more appropriate to a surface diffusion process than to a chemical reaction between as reactive a combination as an oxygen adatom and an active site. Therefore, we believe that the process described by the rate constant k is a surface migration step of the same type observed in the germanium-chlorine reaction.[28]

(3) Activation Energy of Surface Migration

First principles calculations of adatom binding and migration energies usually yield absolute values considerably larger than the experimental results. However, the ratio of the binding and migration energies obtained from such calculations is considered reliable. Bennett et al[29] have recently calculated the energetics of oxygen interactions with graphite. Their calculation yielded the ratio $E/E_d^\circ=0.18$, where E_d° and E denote the binding and migration energies respectively. Applying this ratio to the migration energy determined experimentally in the present study, the binding energy of atomic oxygen on graphite should be $30/0.18\simeq170$ kcal/mole, which is comparable to the 192 kcal/mole strength of the C=O bond.[30] Experimental values of E_d° have been reported as 97 kcal/mole[19] and 110 kcal/mole.[31]

E. Nature of the B Sites

The B sites are not subject to the oxidative generation thermal-annealing balance as are the A sites. If the B sites responded to their environment in the same manner as the A sites,

we would have observed phase hysteresis as well as amplitude hysteresis (inasmuch as the B site density enters into the rate constant k, which appears in the phase lag expression). Because of the absence of phase hysteresis, we conclude that the B site density either is unaffected by temperature variations or it responds essentially instantaneously to changes in surface temperature (in the latter case, the temperature dependence of N_B is added to that of D_S). We suspect that the most likely explanation is the one used in determining N_B, namely that the B site density is temperature independent. The site density of $\sim 10^9 cm^{-2}$ and the apparent resistance of B sites to any environmental influence suggests that these centers may represent the termination of dislocation lines at the surface of the graphite specimen. The targets are subject to severe thermal stresses, so that the rather large number of dislocations per unit area is not surprising. The enhanced reactivity to oxidation of the surface where screw dislocations emerge has been noted by Thomas and Roscoe.[32]

We visualize that an oxygen adatom may form a bound CO on any carbon atom in the highly distorted region of a dislocation core. The binding of an oxygen adatom by a carbon atom within this region does not prevent other carbon atoms in the same region from being active. This property is different from the behavior of the A sites which, although large (σ=75Å), are incapacitated by chemisorption of a single O_2 molecule. The strained area surrounding an emerging dislocation line may be quite large, so that the B site, which encompasses this area, cannot be saturated by bound CO. Even though the density of B sites is ~400 times smaller than that

of A sites, if each B site contains more than 400 active carbon atoms, the capacity of the B sites for bound CO is greater than that of the A sites. Reaction ceases by saturation of A sites before the B sites are saturated. Therefore, a B-site coverage dependence has not been included in the kn' rate terms in Eqs(4) and (6).

The B sites are thus believed to be large islands of carbon atoms capable of reacting with adsorbed oxygen atoms but incapable of dissociating impinging oxygen molecules. These islands, although large enough to contain hundreds of carbon atoms, are sufficiently widely separated that surface migration to them constitutes a measurable time lag in the oxidation process even at high temperatures.

F. The Desorption Rate Constant for Bound CO

The measured frequency factor for the CO desorption step ($3 \times 10^{12} sec^{-1}$) is in good agreement with values observed for many systems.[33]

The measured activation energy of 50 kcal/mole for this step may be compared to the independent measurement of the heat of adsorption of CO or freshly prepared graphite surfaces, which is 42 kcal/mole.[31]

It seems quite clear that the desorption step has been properly described by the reaction model.

G. Comparison of Lock-in Amplifier Results with Analysis of the Complete Waveform

As discussed in Part I of this series, direct measure-

ment of the product signal waveform is an alternative to the treatment of the signal by the lock-in amplifier. In order to ascertain that these two methods are consistent, the following experiment was undertaken. A digital signal-to-noise averager was used to recover the CO output signal directly from the mass spectrometer during a modulated beam experiment. The surface was at 1175°K and the modulation frequency was 16 Hz. Fig. 15 shows the scattered reactant beam profile and the desorbed CO reaction product signal along with two curves fit to the data points. The curves have been normalized to the data points at the end of the "on" and "off" portions of the modulation cycle.

The solid curves represent a plot of n_A+n_B according to Eqs(7)-(12), with the values of the constants determined by the preceeding analysis. Since the modulated signal is proportional to the product emission rate from the surface, which in turn is proportional to the surface concentration of bound CO, the data points of Fig. 15 may be compared directly to theoretical predictions of $n_A(t)+n_B(t)$.

The dashed curve of Fig. 15 represents a single exponential fit to the data accumulated by the digital signal averager. The form chosen was:

$$n_{ON}(t) = 1 - e^{-Ct}$$

$$n_{OFF}(t) = e^{-Ct}$$

Because of the scatter of the points in Fig. 15 (which could be reduced by a longer data accumulation period), it is not obvious

that Eqs(7)-(12) of the proposed reaction model provide a better description of the waveform than the simple single exponential function. However, the data of Fig. 15 and single exponential fits to waveform measurements at two other temperatures showed that the fitting parameter C had an unreasonably low activation energy of 7 kcal/mole. Thus, any reaction model which has but one characteristic reaction time does not provide meaningful kinetic parameters. These results again indicate the need for a two-branch mechanism to describe the basal plane oxidation process.

H. Annealed Pyrolytic Graphite

A target fabricated from the annealed pyrolytic graphite in the basal plane orientation was tested in a manner similar to the as-received material used for the bulk of this investigation. Practically no CO signal was observed at any temperature. The reaction probability on the annealed material is barely at the limit of system sensitivity, which at mass 44 is $\sim 2 \times 10^{-5}$. Heat treatment apparently makes a vast difference in the reactivity of pyrolytic graphite.

Table 1

Impurity Content of Oxygen

Species	Concentration, ppm
N_2	4
CO_2	3
CO	0
H_2	0
He	0
Ne	0
Kr	4
Xe	1
Hydrocarbons	0

LITERATURE CITED

1. R. Jones, D.R. Olander, W. Siekhaus and J.A. Schwarz, Part I of this series.

2. I. Langmiur, J. Am. Chem. Soc. 37, 1139 (1915).

3. X. Duval, Ann. Chim., Ser. 12, Vol. 10, 905 (1955).

4. J. Nagle and R.F. Strickland-Constable, Proc. of the Fifth Conf. on Carbon, Vol. 1 (Pergamon Press, 1962) p. 154.

5. J.R. Walls and R.F. Strickland-Constable, Carbon 1, 333 (1964).

6. G. Blyholder, J.S. Binford, and H. Eyring, J. Phys. Chem. 62, 263 (1958).

7. D.E. Rosner and H.D. Allendorf, AIAA Journal 6, 650 (1968).

8. N.R. Laine, F.J. Vastola, and P.L. Walker, Jr., Proc. of the Fifth Conf. on Carbon, Vol. 2 (Pergamon Press, 1963) p. 211.

9. R.O. Lussow, F.J. Vastola, and P.L. Walker, Jr., Carbon 5, 591 (1967).

10. F.J. Vastola, P.J. Hart and P.L. Walker, Jr., Carbon 2, 65 (1964).

11. G.R. Hennig, Proc. of the Fourth Conf. on Carbon (Pergamon Press, 1960) p. 145.

12. G.R. Hennig, Proc. of the Fifth Conf. on Carbon, Vol. 1 (Pergamon Press, 1962) p. 143.

13. G.R. Hennig and M.A. Kanter, Fourth Int. Symp. on the Reactivity of Solids, Amsterdam (1960) p. 648, J.H. deBoer, ed.

14. J.M. Thomas and C. Roscoe, Chemistry and Physics of Carbon, Vol. 3, P.L. Walker, Jr., ed., Marcel Dekker, New York (1968) p. 1.

15. J.M. Thomas, ibid., Vol. 1 (1965), p. 121.

16. F.S. Feates, Carbon, 6, 949 (1968).

17. R.A. Krakowski and D.R. Olander, J. Chem. Phys. 49, 5027 (1968).

18. R.E. Stickney and J.C. Batty, J. Chem. Phys. 51, 4475 (1969).

19. H.I. Bull, M.H. Hall, and W.E. Garner, J. Chem. Soc. (London) 837 (1931).

20. P. Kisliuk, J. Phys. Chem. Solids, 3, 95 (1957).

21. P. Kisliuk, J. Phys. Chem. Solids, 5, 78 (1958).

22. J.A. Becker and C.D. Hartman, J. Phys. Chem. 57, 157 (1953).

23. G. Ehrlich, J. Phys. Chem. 60, 1338 (1956).

24. D.R. Olander, Proc. of the Fourth Intern. Materials Symp. (Wiley, 1969)pp. 45-1 to 45-50, G.A. Somorjai, ed.

25. R. Jones, Ph.D. Thesis, AEC Report LBL-104 (1971).

26. F.M. Wachi and D.E. Gilmartin, Carbon 8, 141 (1970).

27. P. Beckmann, IEEE Trans. on Antennas and Propagation, AP-13, 384 (1965).

28. R.J. Madix and J.A. Schwarz, Surf. Sci. 24, 264 (1971).

29. A.J. Bennett, B. McCarroll, and R.P. Messmer, Phys. Rev. B3, 1397 (1971).

30. H.S. Johnston, Gas Phase Reaction Rate Theory, Ronald Press, New York (1966), p. 78.

31. Yu. A. Zarifyanz, V.F. Kiselev, N.N. Lezhnev, and O.V. Nikitina, Carbon, 5, 127 (1967).

32. J.M. Thomas and C. Roscoe, J. Nucl. Mater. 15, 235 (1965).

33. G. Ehrlich, Transactions of the Eighth Vacuum Symposium, Pergamon Press (1962), p. 126.

FIGURE CAPTIONS

1. Effect of target temperature on the apparent reaction probability of CO

2. Variation of CO phase lag with target temperature

3. Four hysteresis loops

4. Decay of the CO signal following increase of the target temperature

5. Effect of "cooking" the specimen at 1125°K with the molecular beam either on or off

6. Kinetic order plots for CO at various temperatures

7. Variation of CO signal with temperature of the oxygen molecular beam

8. Frequency scan at 1305°K - CO phase lag

9. Frequency scan at 1305°K - CO apparent reaction probability

10. Apparent reaction probability of CO_2

11. Kinetic order plot for CO_2

12. Plot to determine the rate constant k from high temperature phase lag measurements. Error bars represent the estimated ±1° precision of the phase angle measurements

13. Comparison of CO apparent reaction probability with theory

14. Scanning electron micrographs basal plane specimens of unannealed pyrolytic graphite. Top: after polishing; Bottom: after extensive oxidation by the molecular beam

15. Waveform of the CO product signal obtained by a digital signal-to-noise averager. T_s=1175°K, 16 Hz

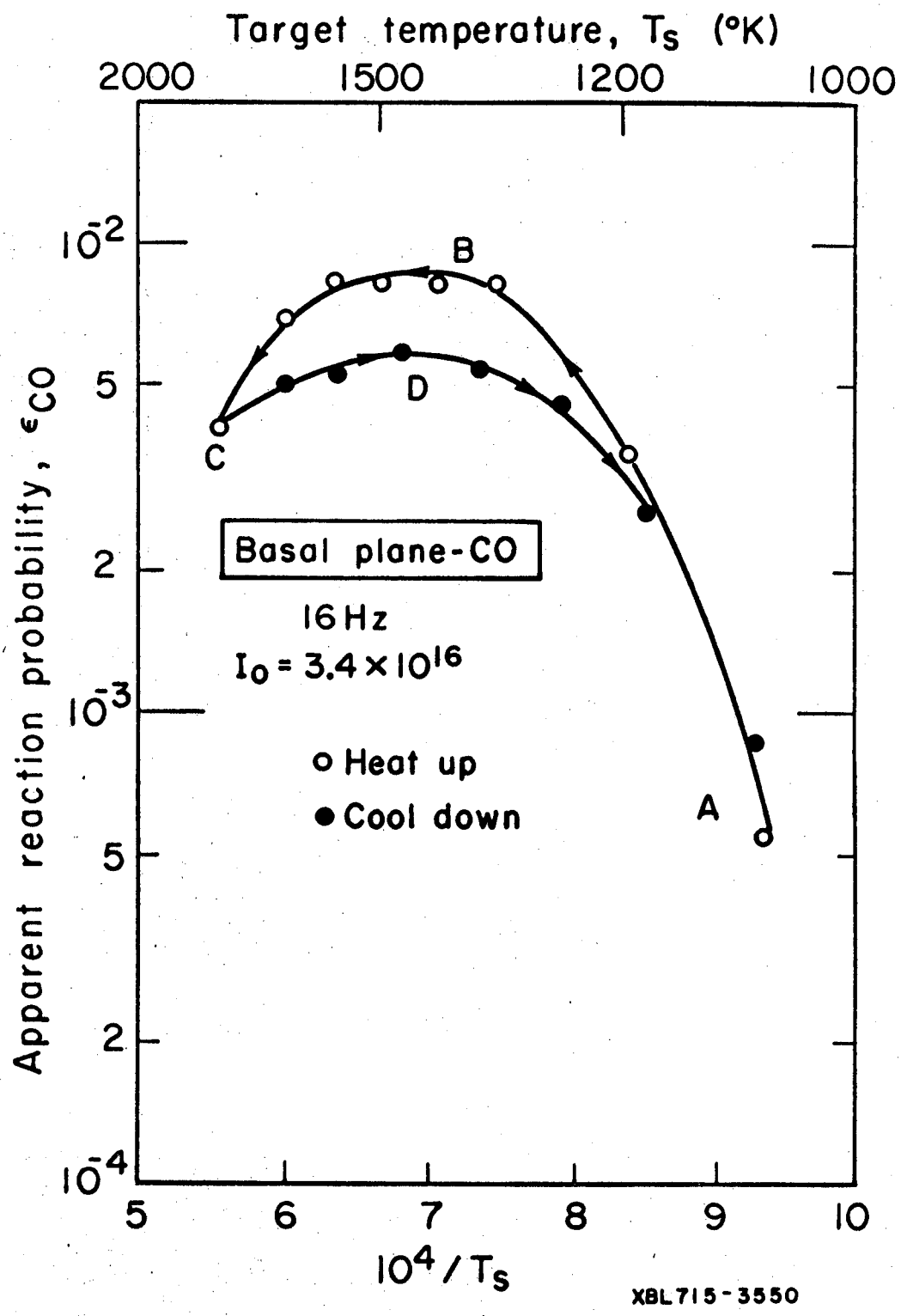
Target temperature, T_s (°K)
2000
1500
1200
1000
10^{-2}
5
2
10^{-3}
5
2
10^{-4}
Apparent reaction probability, ϵ_{CO}
B
D
C
A
Basal plane-CO
16 Hz
$I_o = 3.4 \times 10^{16}$
o Heat up
● Cool down
5
6
7
8
9
10
$10^4 / T_s$
XBL715-3550

Fig. 1

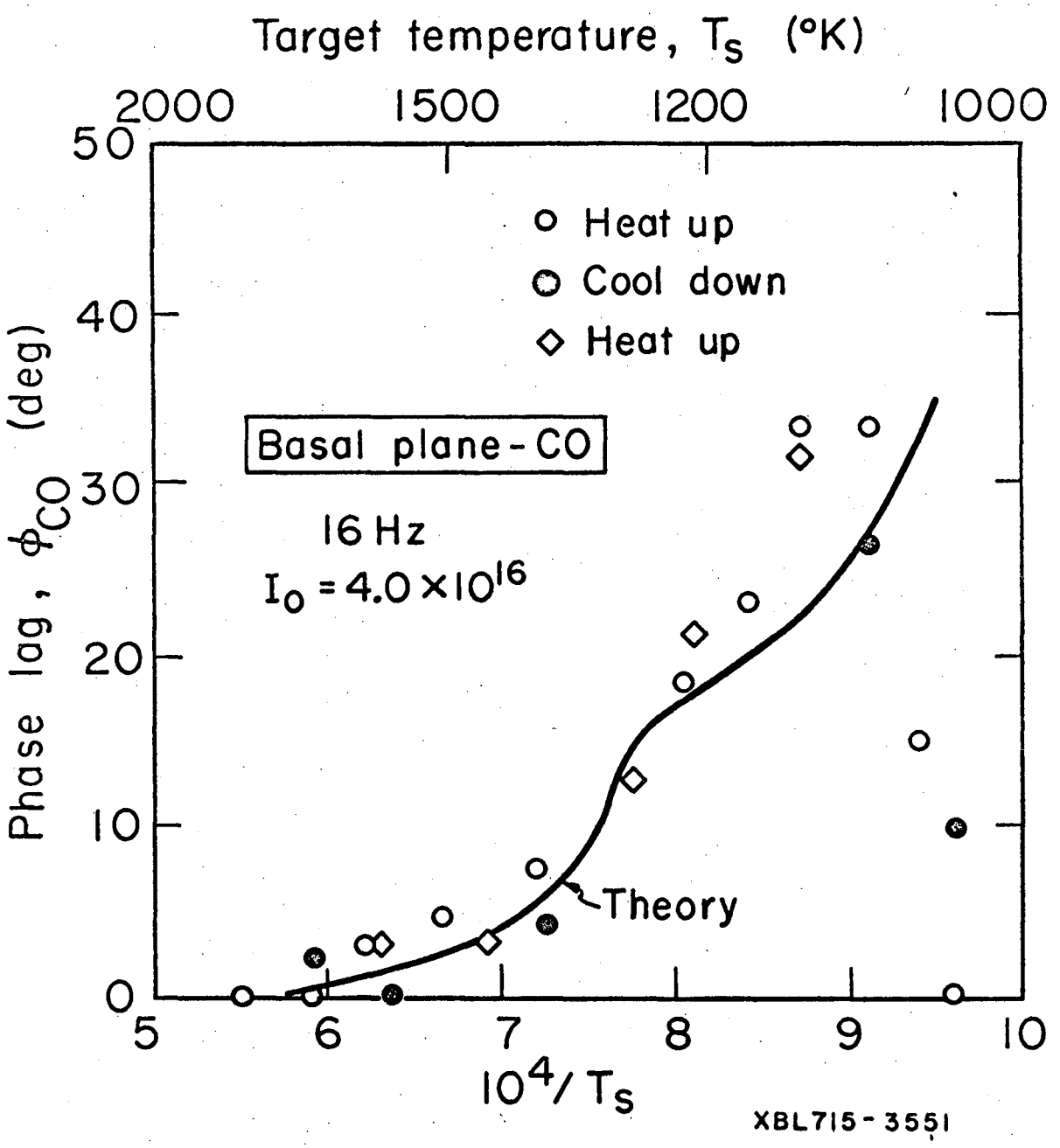
Target temperature, T_s (°K)
2000
1500
1200
1000
50
40
30
20
10
0
Phase lag, ϕ_{CO} (deg)
Heat up
Cool down
Heat up
Basal plane - CO
16 Hz
$I_o = 4.0 \times 10^{16}$
Theory
5
6
7
8
9
10
$10^4 / T_s$
XBL715-3551

Fig. 2

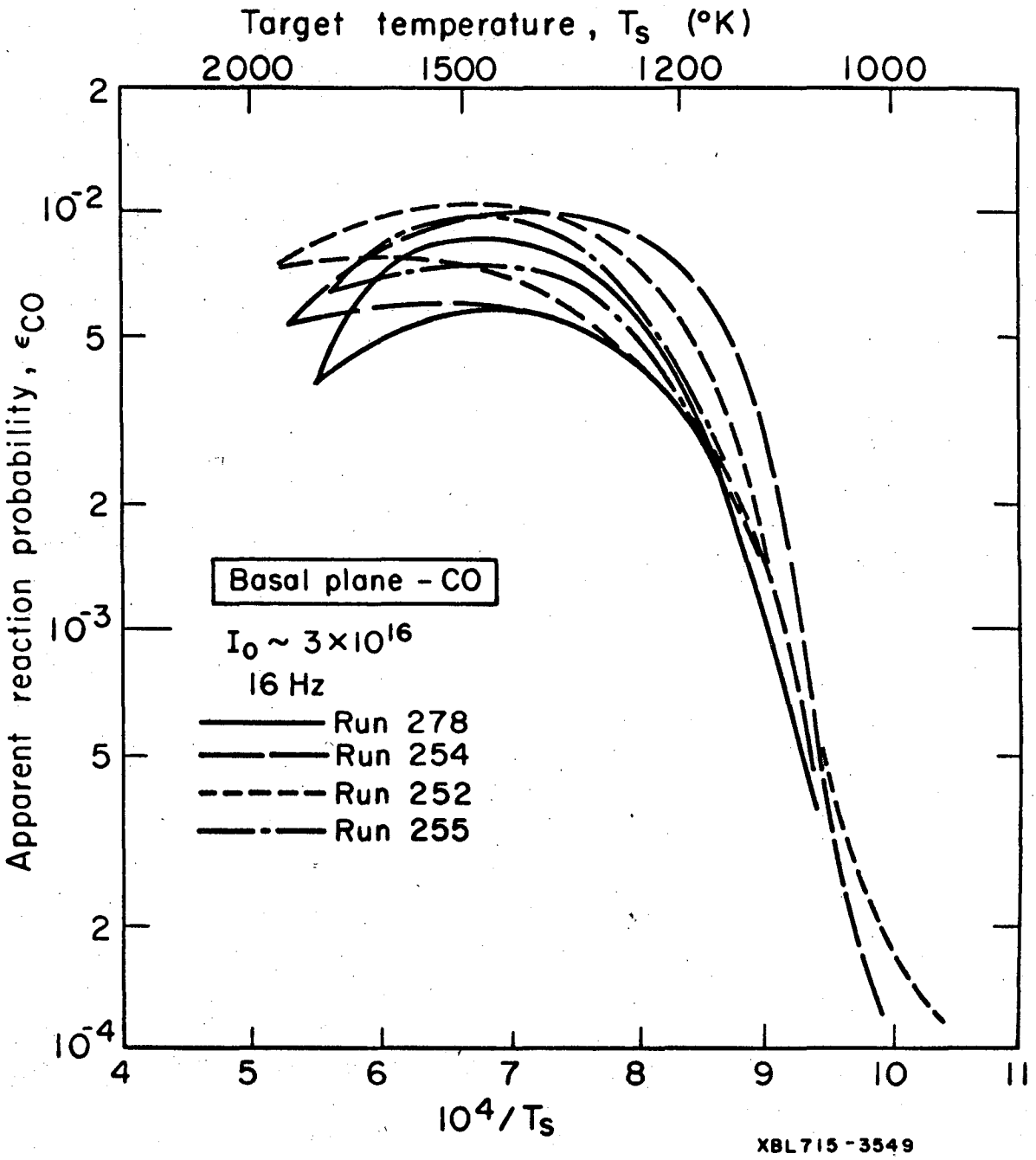
Target temperature, T_s (°K)
2000
1500
1200
1000
Apparent reaction probability, ϵ_{CO}
10^{-2}
10^{-3}
10^{-4}
Basal plane - CO
$I_0 \sim 3 \times 10^{16}$
16 Hz
Run 278
Run 254
Run 252
Run 255
4
5
6
7
8
9
10
11
$10^4/T_s$
XBL715-3549

Fig. 3

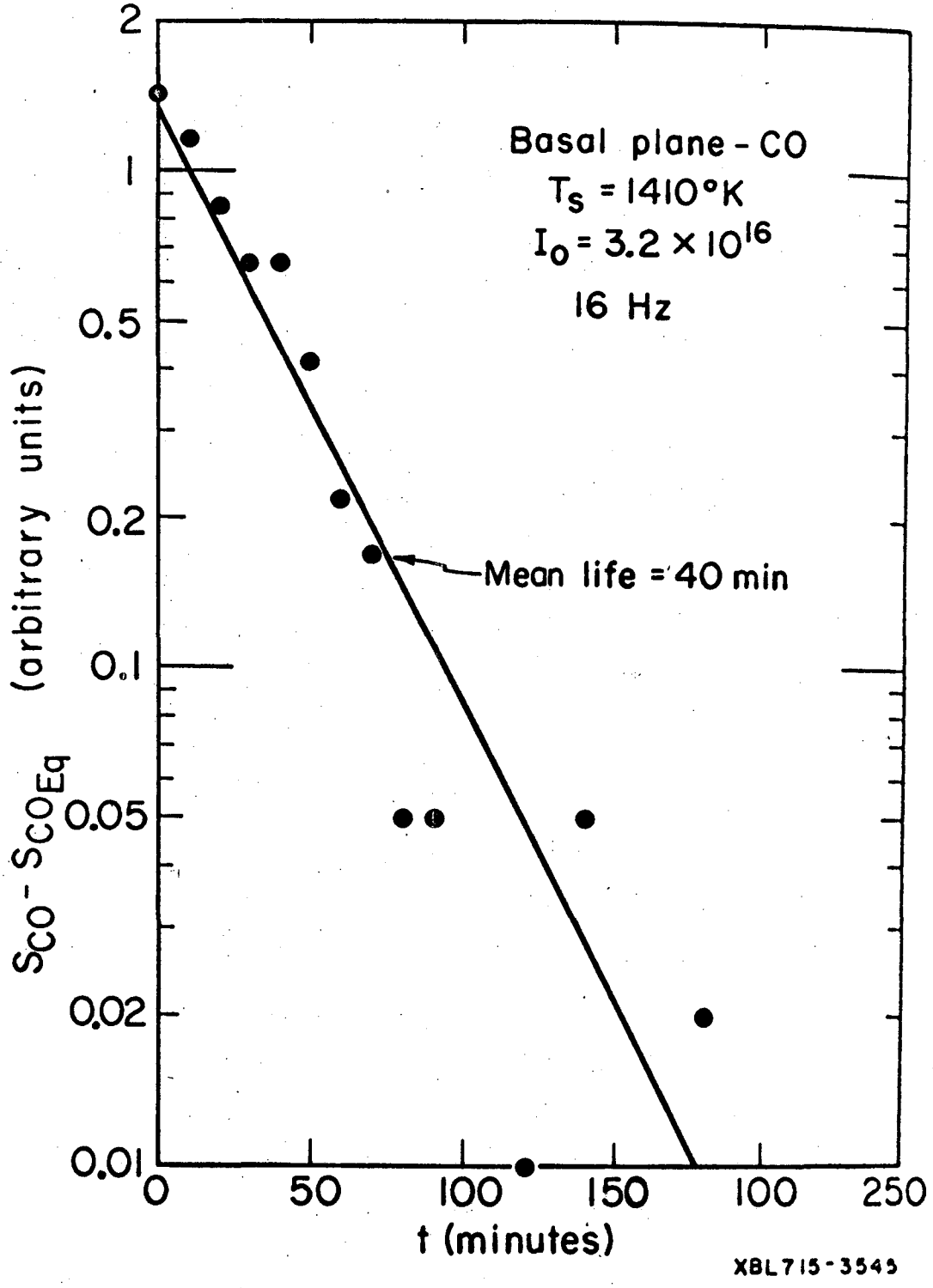
Basal plane - CO
T_s = 1410°K
$I_0 = 3.2 \times 10^{16}$
16 Hz
Mean life = 40 min
$S_{CO} - S_{CO_{Eq}}$ (arbitrary units)
t (minutes)
2
1
0.5
0.2
0.1
0.05
0.02
0.01
0
50
100
150
100
250
XBL715-3545

Fig. 4

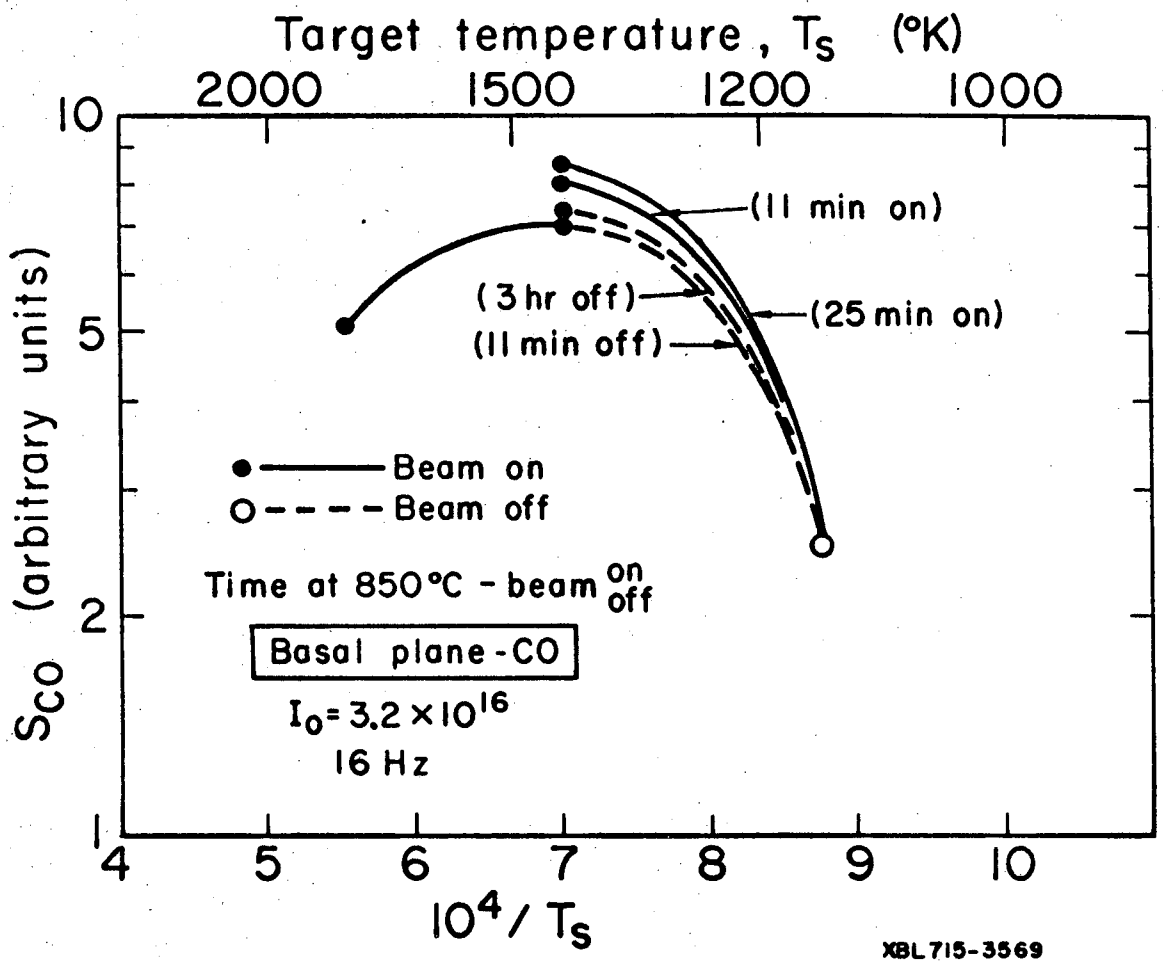
Target temperature, T_S (°K)
2000
1500
1200
1000
10
5
2
1
S_{CO} (arbitrary units)
(11 min on)
(3 hr off)
(11 min off)
(25 min on)
Beam on
Beam off
Time at 850°C - beam on off
Basal plane - CO
$I_0 = 3.2 \times 10^{16}$
16 Hz
4
5
6
7
8
9
10
$10^4 / T_S$
XBL715-3569

Fig. 5

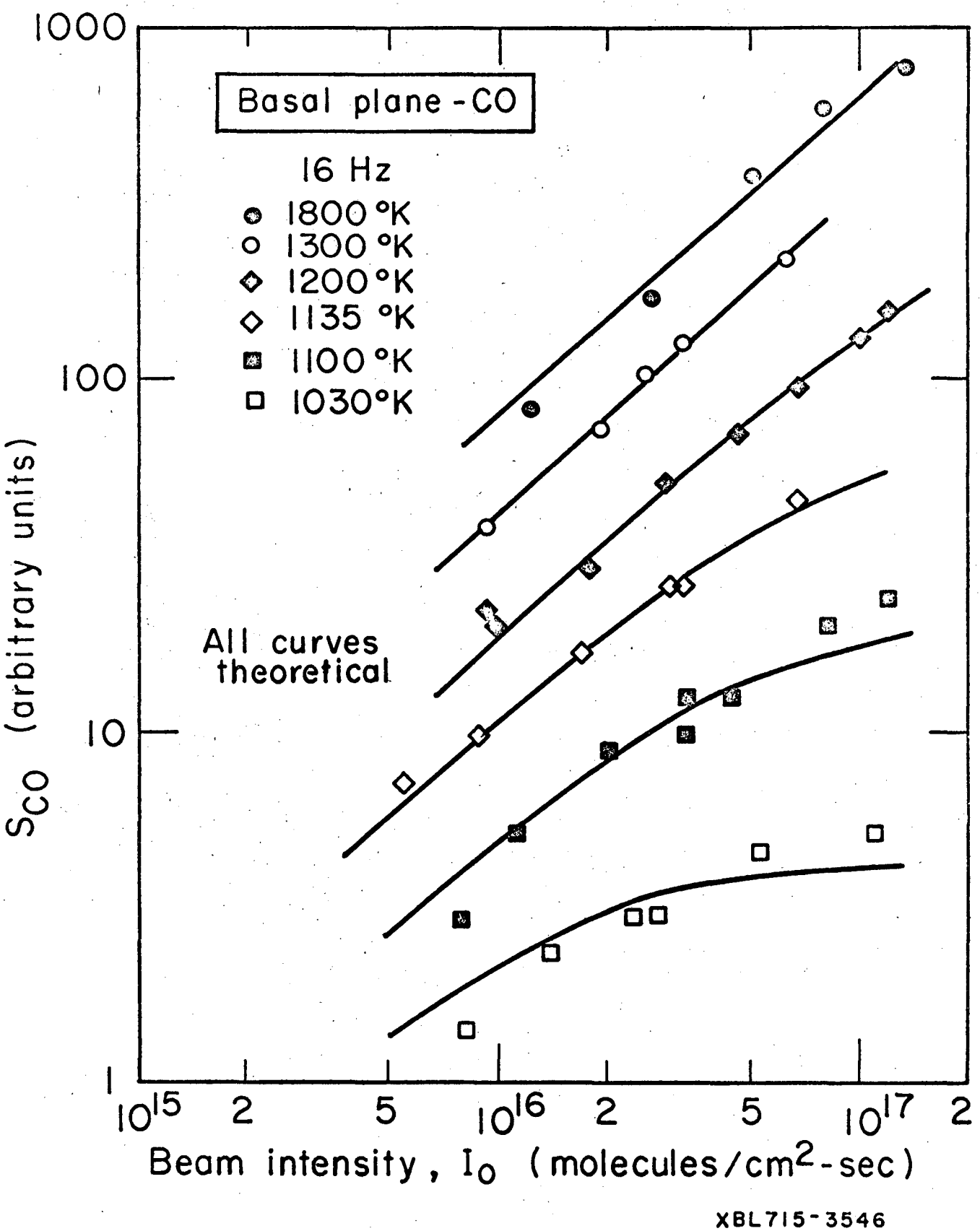
Basal plane - CO
16 Hz
1800 °K
1300 °K
1200 °K
1135 °K
1100 °K
1030°K
All curves theoretical
1000
100
10
1
S_{CO} (arbitrary units)
10^{15} 2 5 10^{16} 2 5 10^{17} 2
Beam intensity, I_o (molecules/cm^2-sec)
XBL715-3546

Fig. 6

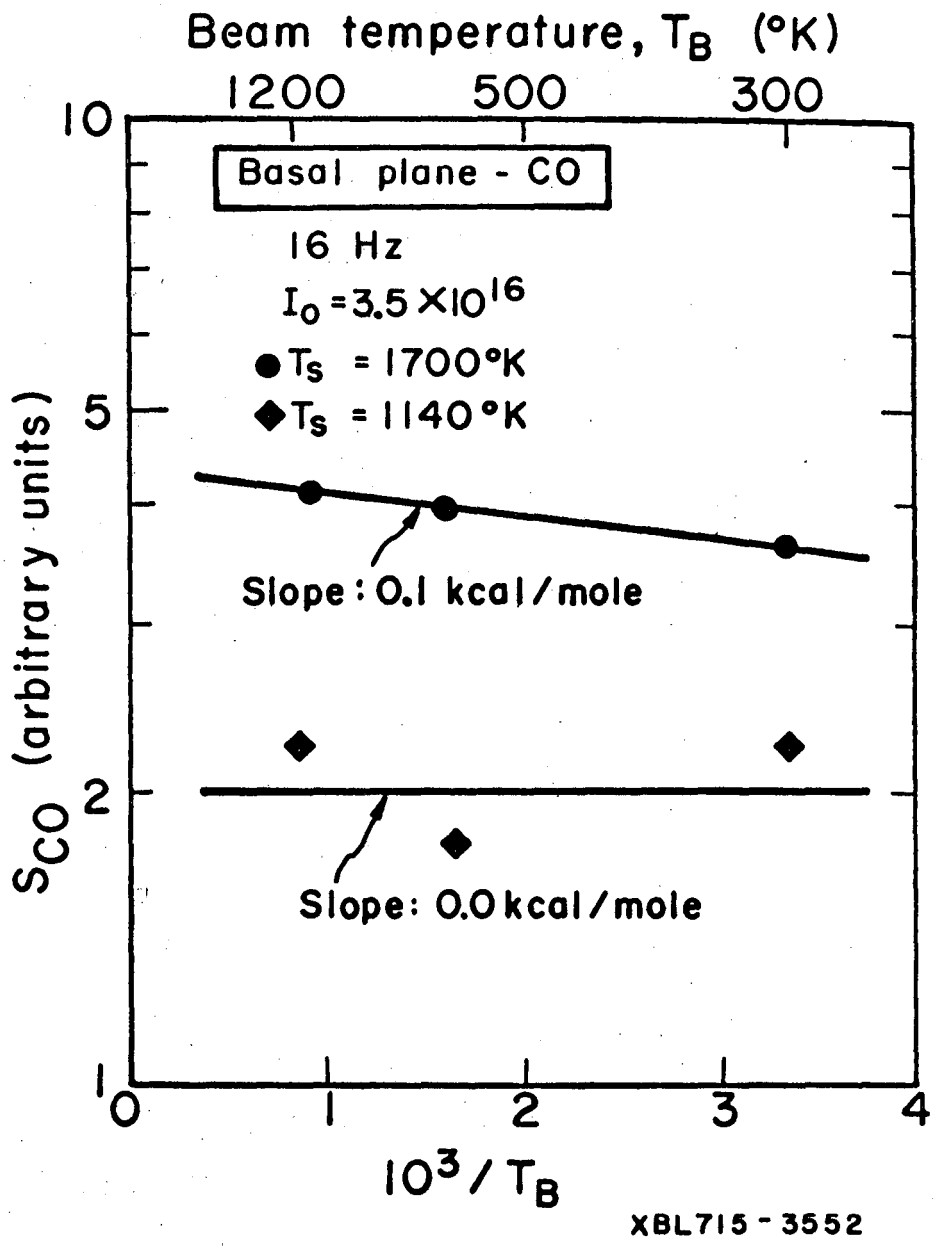
Beam temperature, T_B (°K)
1200
500
300
10
5
2
1
Basal plane - CO
16 Hz
$I_0 = 3.5 \times 10^{16}$
● T_s = 1700°K
◆ T_s = 1140°K
Slope: 0.1 kcal/mole
Slope: 0.0 kcal/mole
S_{CO} (arbitrary units)
0
1
2
3
4
$10^3 / T_B$
XBL715-3552

Fig. 7

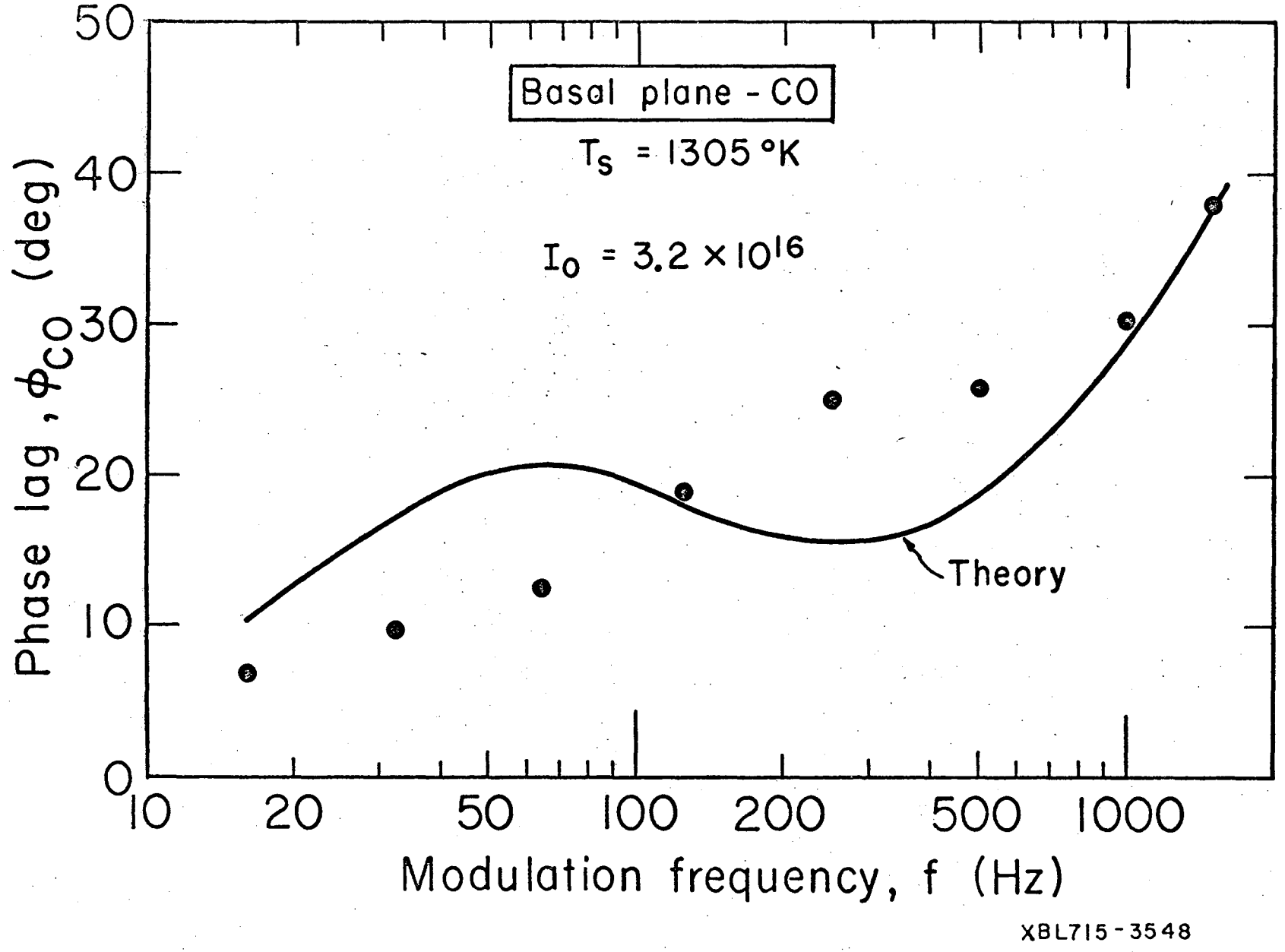
Basal plane - CO
T_s = 1305 °K
I_o = 3.2 × 10^16
Theory
Phase lag, ϕ_{CO} (deg)
Modulation frequency, f (Hz)
0
10
20
30
40
50
10
20
50
100
200
500
1000
XBL715-3548

Fig. 8

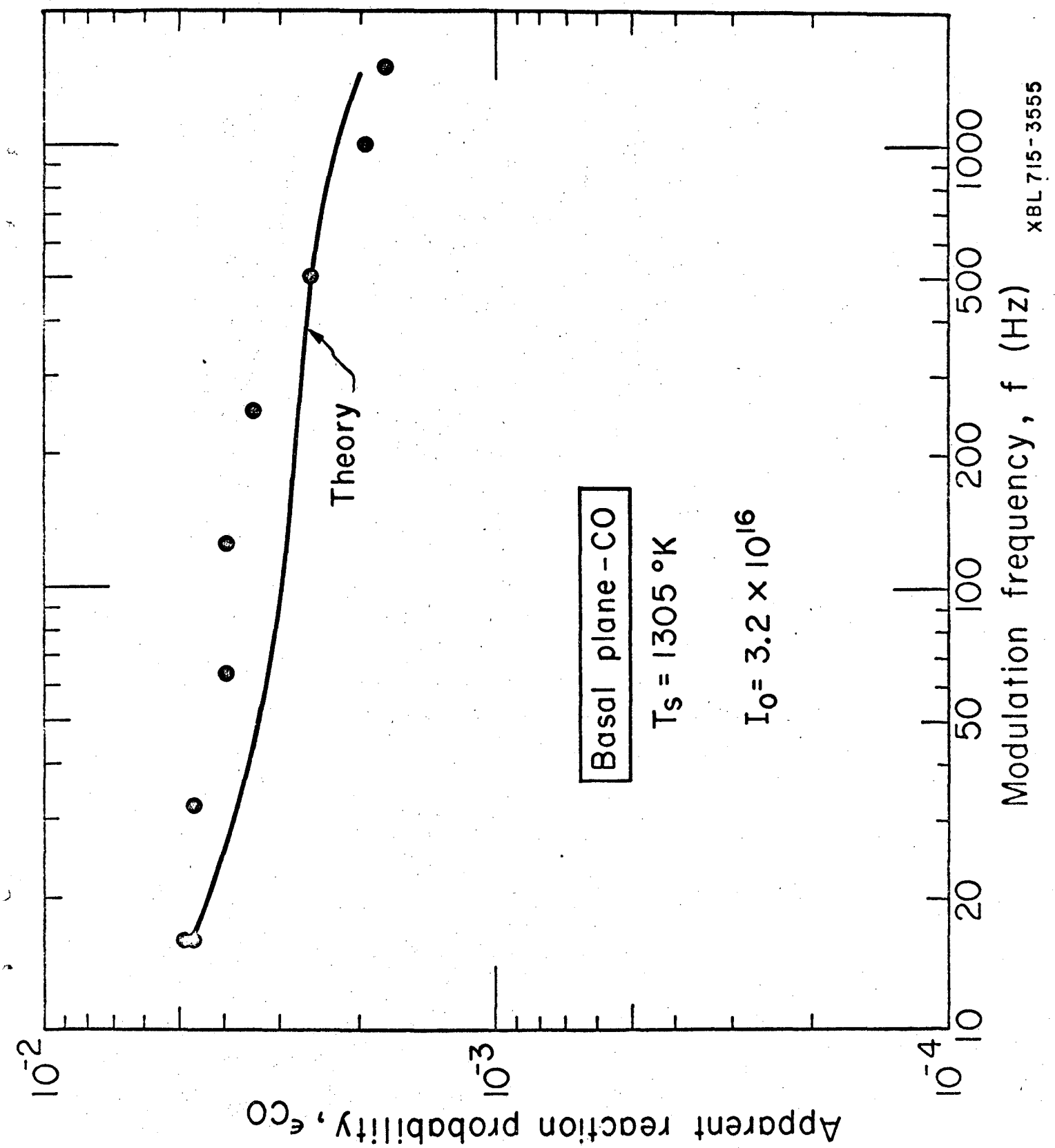
Apparent reaction probability, ϵ_{CO}
10^{-2}
10^{-3}
10^{-4}
10
20
50
100
200
500
1000
Modulation frequency, f (Hz)
XBL 715-3555
Theory
Basal plane-CO
T_s = 1305 °K
I_o = 3.2 x 10^{16}

Fig. 9

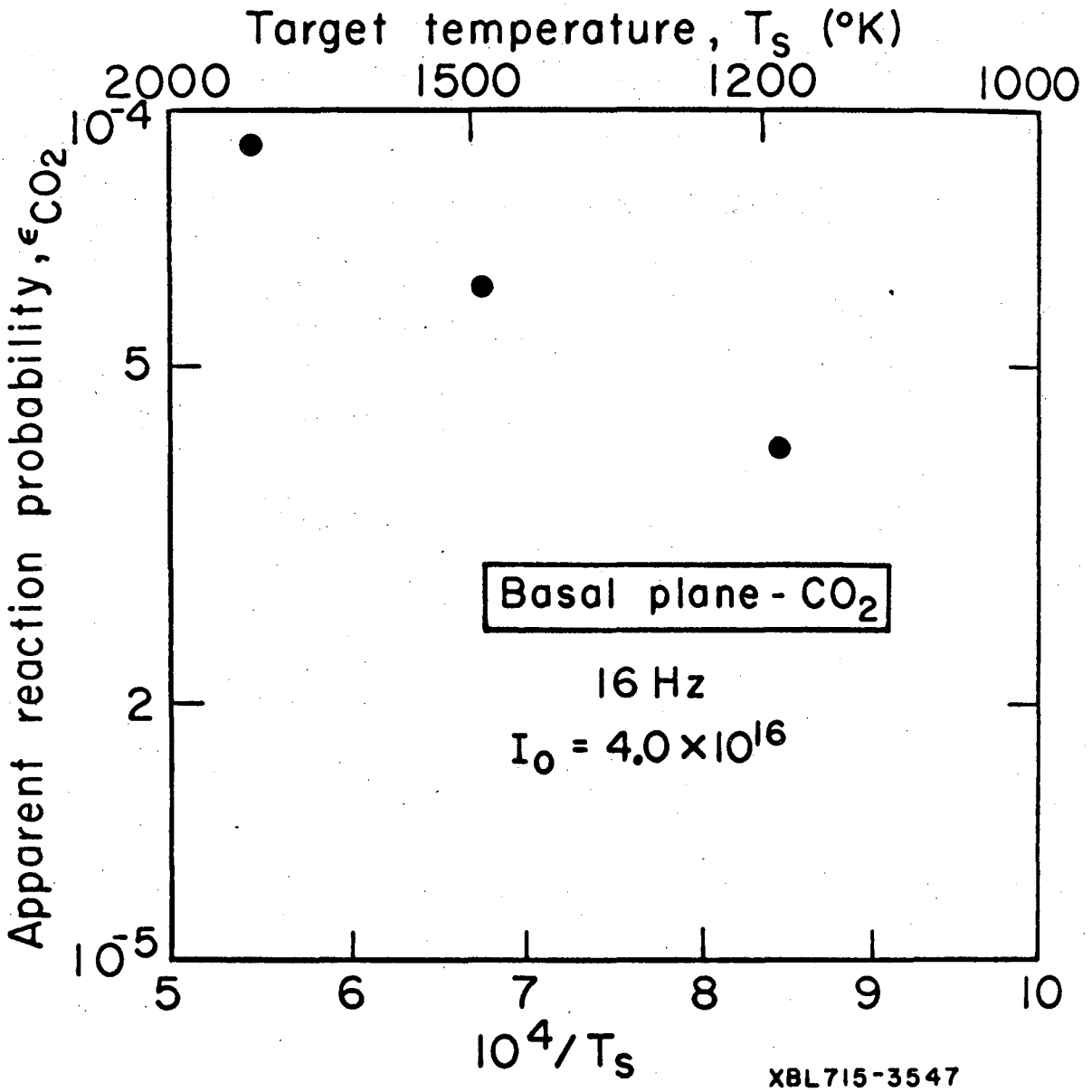
Target temperature, T_s (°K)
2000
1500
1200
1000
Apparent reaction probability, ϵ_{CO_2}
10^{-4}
5
2
10^{-5}
Basal plane - CO_2
16 Hz
$I_o = 4.0 \times 10^{16}$
5
6
7
8
9
10
$10^4/T_s$
XBL715-3547

Fig. 10

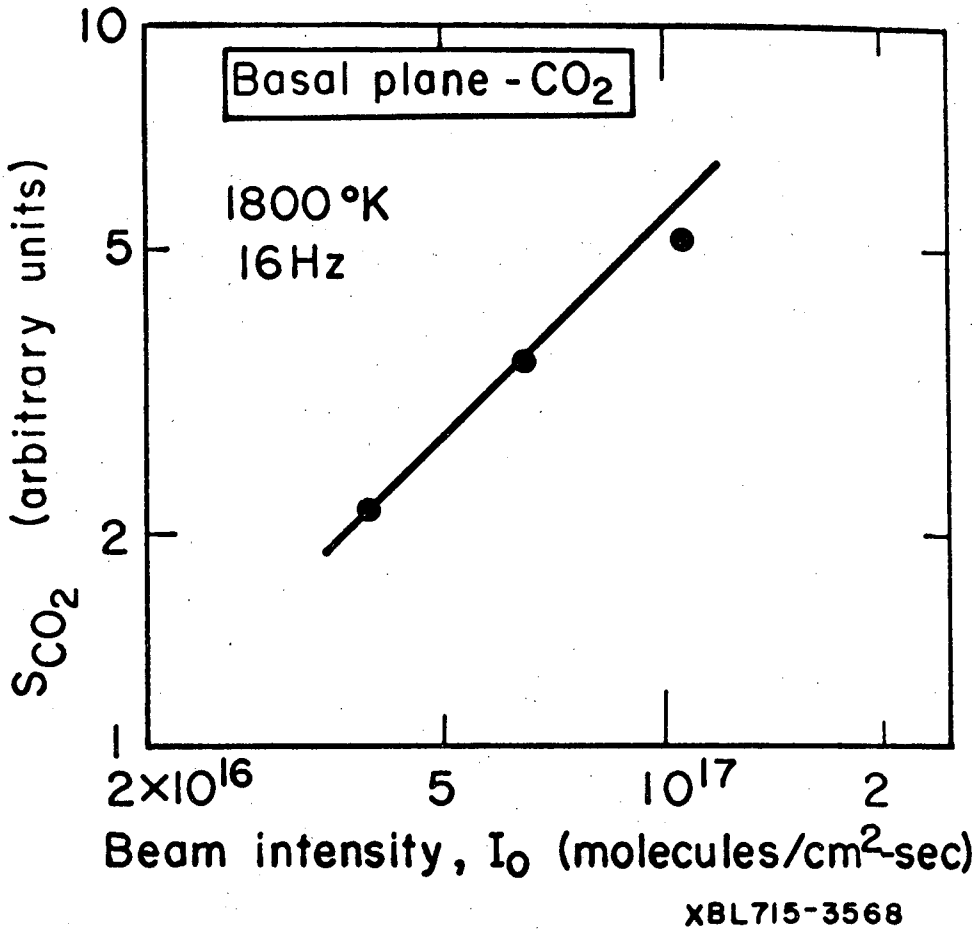
Basal plane - CO_2
1800 °K
16 Hz
S_{CO_2} (arbitrary units)
10
5
2
1
2×10^{16}
5
10^{17}
2
Beam intensity, I_0 (molecules/cm^2-sec)
XBL715-3568

Fig. 11

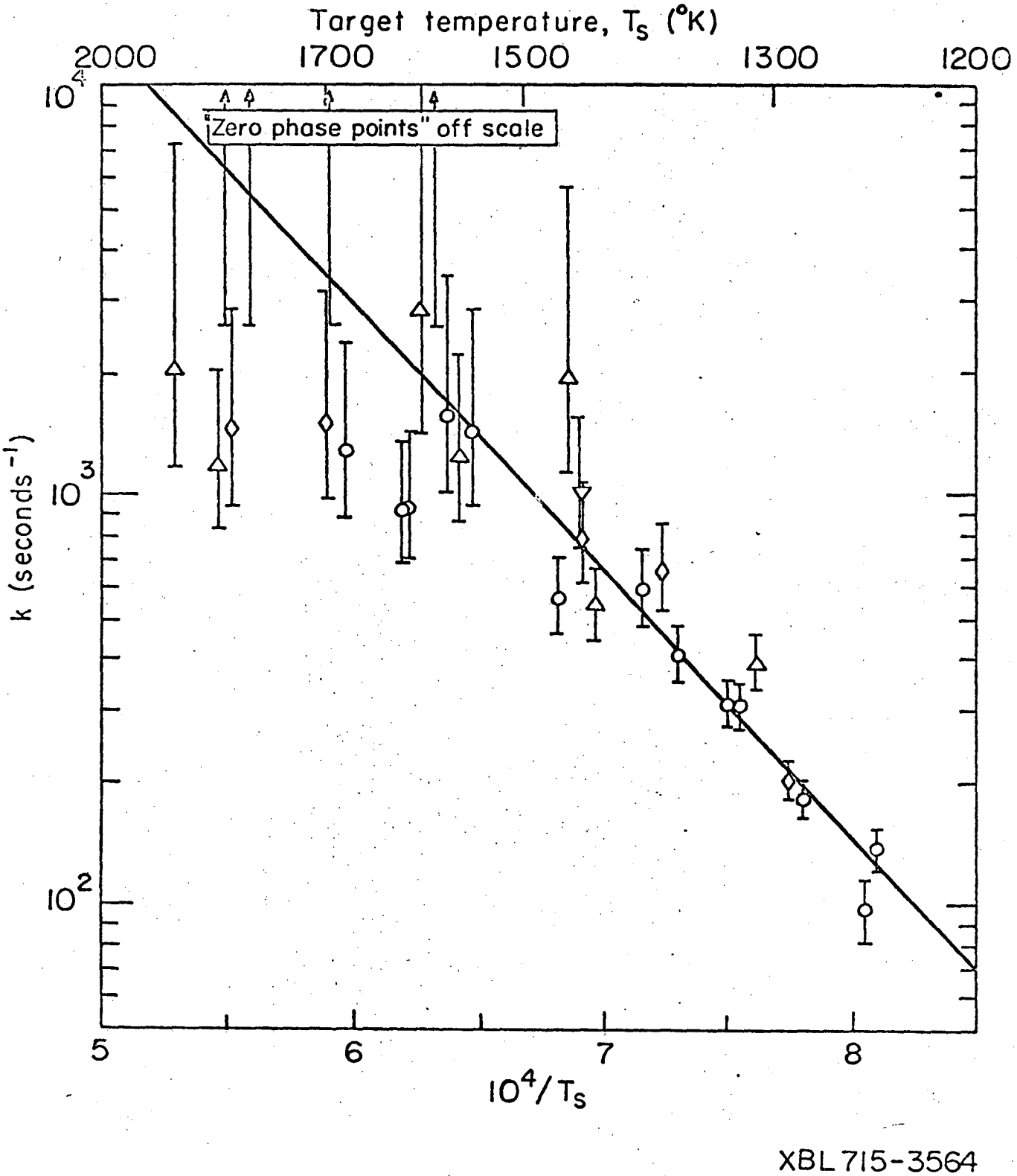
Target temperature, T_s (°K)
2000
1700
1500
1300
1200
"Zero phase points" off scale
k (seconds^{-1})
10^4
10^3
10^2
5
6
7
8
$10^4/T_s$
XBL715-3564

Fig. 12

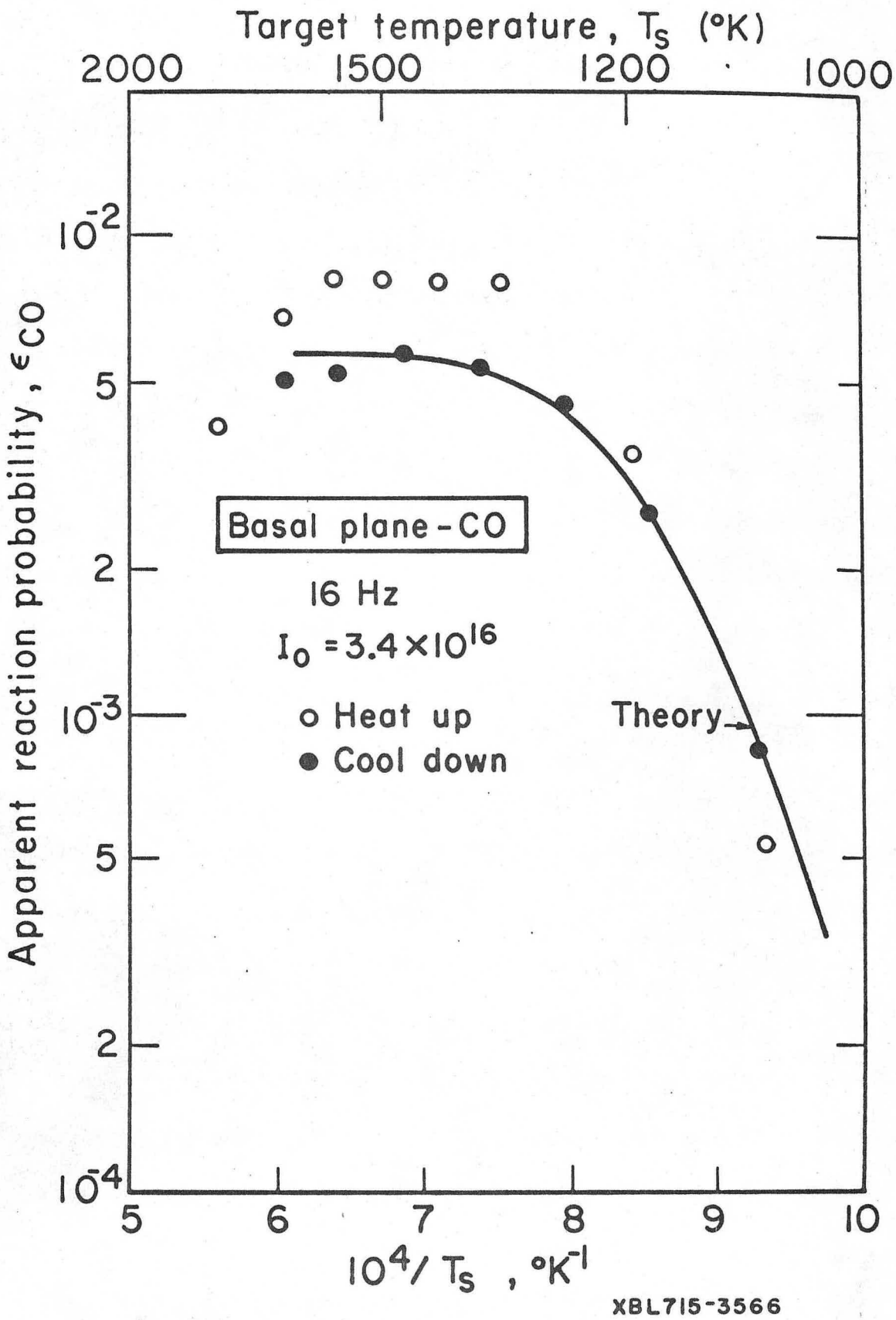
Target temperature, T_s (°K)
2000
1500
1200
1000
Apparent reaction probability, ϵ_{CO}
10^{-2}
5
2
10^{-3}
5
2
10^{-4}
Basal plane - CO
16 Hz
$I_0 = 3.4 \times 10^{16}$
o Heat up
● Cool down
Theory
5
6
7
8
9
10
$10^4 / T_s$, °K^{-1}
XBL715-3566

Fig. 13

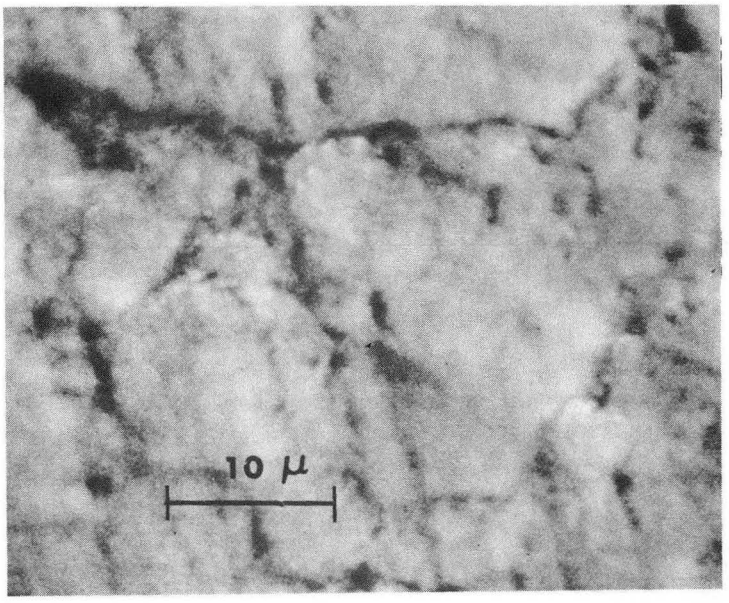

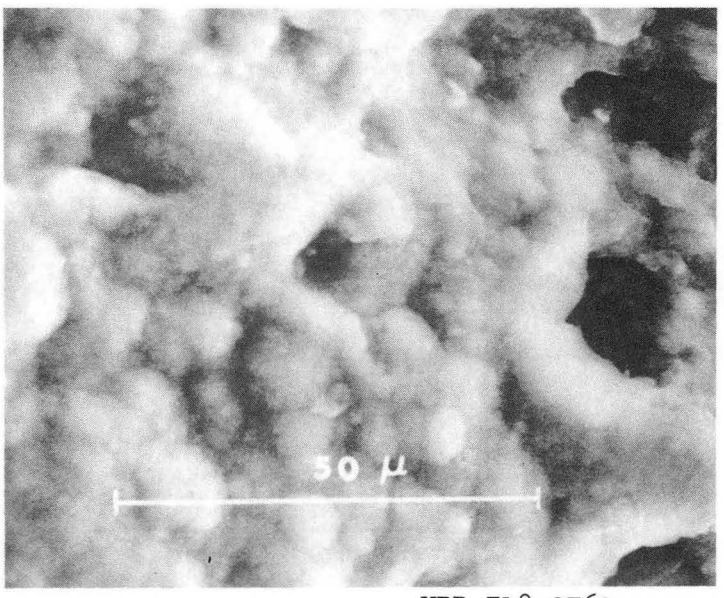

XBB 718-3769

Fig. 14

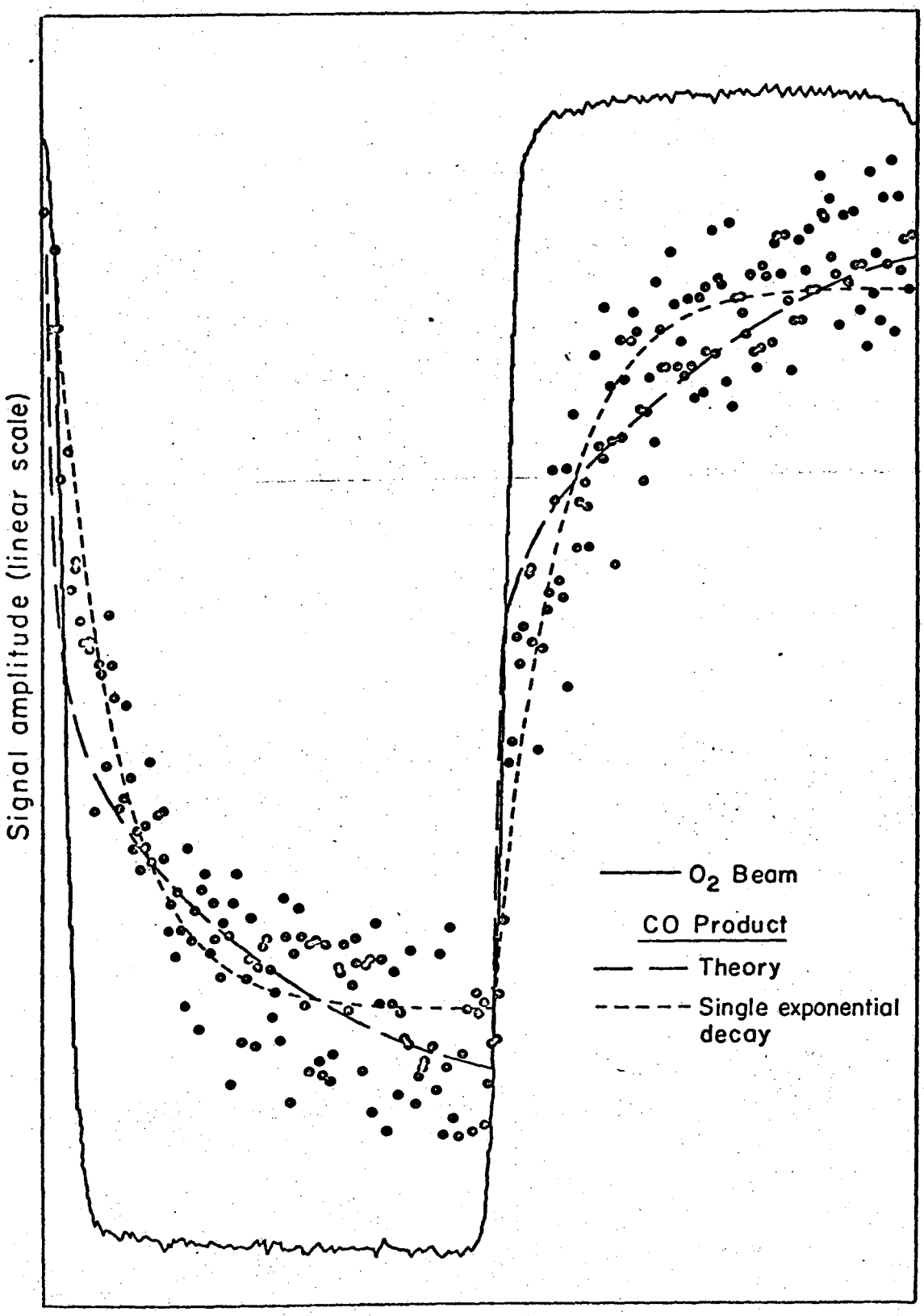

Fig. 15

XBL719-7315

TECHNICAL INFORMATION DIVISION
LAWRENCE BERKELEY LABORATORY
UNIVERSITY OF CALIFORNIA
BERKELEY, CALIFORNIA 94720